Front. Mater. Sci.
DOI 10.1007/s11706-012-0170-8

REVIEW ARTICLE

Resistive switching effects in oxide sandwiched structures

Xiao-Jian ZHU[1,2], Jie SHANG[1,2], and Run-Wei LI (✉)[1,2]

1 Key Laboratory of Magnetic Materials and Devices, Ningbo Institute of Materials Technology and Engineering (NIMTE), Chinese Academy of Sciences (CAS), Ningbo 315201, China
2 Zhejiang Province Key Laboratory of Magnetic Materials and Application Technology, Ningbo Institute of Materials Technology and Engineering (NIMTE), Chinese Academy of Sciences (CAS), Ningbo 315201, China

© Higher Education Press and Springer-Verlag Berlin Heidelberg 2012

ABSTRACT: Resistive switching (RS) behaviors have attracted great interest due to their promising potential for the data storage. Among various materials, oxide-based devices appear to be more advantageous considering their handy fabrication and compatibility with CMOS technology, though the underlying mechanism is still controversial due to the diversity of RS behaviors. In this review, we focus on the oxide-based RS memories, in which the working mechanism can be understood basically according to a so-called filament model. The filaments formation/rupture processes, approaches developed to detect and characterize filaments, several effective attempts to improve the performances of RS and the quantum conductance behaviors in oxide-based resistive random access memory (RRAM) devices are addressed, respectively.

KEYWORDS: resistive random access memory (RRAM), resistive switching (RS), oxide film, filaments, quantum conductance

Outline

1 Introduction
2 Resistive switching behaviors and filaments formation/rupture processes
3 Detection of filaments
 3.1 Resistance–device area relationship
 3.2 Resistance–temperature character
 3.3 Observation by local current atomic force microscopy
 3.4 Transmission electron microscopy characterization
4 Resistive switching performances enhancement
 4.1 Electrode effects on resistive switching performances
 4.2 Microstructure dependence of resistive switching behaviors
  4.2.1 Crystallization effect
  4.2.2 Oxygen content in oxides
  4.2.3 Doping effect
5 Quantum conductance behaviors in oxide-based resistive random access memories
6 Summary and outlook
Abbreviations
Acknowledgements
References

1 Introduction

Resistive switching (RS) phenomenon was reported first by Hickmott [1] in oxide films in 1960s. Then, extensive researches intended to reveal the intrinsic mechanism of the RS and developed their applications were performed [2–3]. In 2000, Liu et al. reported an observation of RS behaviors in $Pr_{0.7}Ca_{0.3}MnO_3$ (PCMO) films [4]. Subsequently, in a large variety of materials including organic materials [5–6],

Received May 6, 2012; accepted May 24, 2012

E-mail: runweili@nimte.ac.cn

amorphous silicon (a-Si) [7–8], carbon-based materials [9–11], binary oxides such as NiO [12–14], ZrO_2 [15–16] and HfO_2 [17–19] as well as complex oxides such as $Pr_{1-x}Ca_xMnO_3$ [20–21], $BiFeO_3$ (BFO) [22–24], and $SrTiO_3$ [25–27] were found to exhibit RS behaviors under electrical modulations. For applications, the observed RS effects are being developed into a new generation nonvolatile resistive random access memory (RRAM) which is considered as a competitive candidate against other promising next-generation nonvolatile memories such as ferroelectric random access memory (FeRAM) [28], magnetic random access memory (MRAM) [29] and phase-change random access memory (PRAM) [30]. RRAM has its own unique advantages such as a simple sandwiched structure as well as excellent properties including lower power consumption, higher write/erase speed, good endurance and especially high scalability, which make it favored by many researchers and semiconductor industries [31].

The driving mechanism of RS effects remains unclear till now, though some models have been proposed to understand the RS behaviors. It was proposed that the conductive filament [32], Schottky barrier [33–34], metal-insulator transition [35], current tunneling induced by ferroelectric polarization [36], space charge limited current [37] etc. play very important roles on RS effects in some specific cases. Among these models, conductive filament model has gained much success and is accepted extensively, in which the formation/rupture of local conducting paths/filaments connecting the two-terminal electrodes dominates the RS process.

RRAM based on RS effects is still far away from practical applications so far, due to no materials or structures satisfying all the memory device requirements [38]. From a perspective of application, the basic requirements for the next-generation nonvolatile memory are the high scalability and stability. However, the RRAM devices based on the filaments formation and rupture process are lack of stability though it is of a potential in scalability. In this review, we first discuss the RS behaviors based on filaments formation/rupture and introduce some methods that could be used to detect and characterize these local conductive filaments. Then we focused on the control of the filaments which could help to improve the RS performances including stability in oxide based RRAM devices. In further, the observed quantum conductance behaviors which may lead to ultrahigh density memory applications were discussed.

2 RS behaviors and filaments formation/rupture processes

RRAM device shows a simple metal-insulator-metal (MIM) sandwiched structure. The “M” generally stands for conductive electrode, including metal, metal oxide as well as other good conductors. The “I” denotes the switching matrix, usually insulator or semiconductor. For filament model based RRAMs, a sufficiently high electrical field to induce a soft dielectric breakdown in the dielectric layer which set the device to a conductive state (low resistive state, LRS or “ON state”) labeled as “Forming” process is generally needed to induce the RS. The Forming process corresponds to the first filaments formation process in a pristine film (subsequent reformation/growth of filaments process can be labeled as Set process). An appropriate compliance current is usually needed to prevent the device from being permanent broke down. In this process, a large mount of defects are formed inside the film and form conductive filaments that connect the two terminal electrodes. There are basically two different filament formation mechanisms involving with different major carrier sources that made up filaments: the foreign atoms and the intrinsic defects. The former one mainly relies on the cations from electrode material, for example, Ag and Cu ions from the electrochemically active Ag and Cu anode. These metal elements can be easily oxidized to metal ions followed by drifting from anode toward cathode (usually made of inert materials, such as Pt) through the matrix and then capture electrons and reduced back to metal atoms. With the accumulation of these metal atoms, the filaments will grow parallel to the direction of the applied electrical field. As long as these metal filaments connect the two-terminal electrodes, the device will be switched on [39–40]. The other type is related with the anions, e.g., oxygen ions in oxides [41]. Under a high electrical field, oxygen ions will migrate from the lattice positions, defects like oxygen vacancies are generated by the assistance of thermal effect. This will change the film stoichiometry and lead to an increase of the electronic conductivity of the film at these locations. When these vacancies form local paths/filaments, the device can be switched to the LRS as well. On the other hand, the rupture of filaments which leads to the switch of a device from a LRS to a high resistive state (HRS, or “OFF state”) is labeled as Reset process. Filaments rupture process can also be divided into two classes, involved with electrochemical reaction and thermal effect, respectively. In

devices with filaments composed of electrochemically active elements such as Ag, the filaments rupture is achieved by applying a reversed bias voltage to electrochemically dissolve the filaments, and turn the device to a HRS. A typical feature for this case is that the Reset current is not necessary large than the current. The other way to disrupt the filaments is by introducing a high current flow through the filaments at nanoscale that induces a large amount of Joule-heat in it, which fuse the filaments [42–43]. In this case, the Reset current is always larger than the compliance current in Set process. The difference between the two types of rupture process can be easily distinguished by studying the dependence of Reset process on the operating electrical polarity. For the first class, the Set process and Reset process must happen on reversed bias voltage polarities, and this switching behavior is called bipolar RS. On the other hand, when the Reset process is independent of the electrical polarity, usually the Set and Reset processes occur on the same bias voltage polarity, the characteristics is named as unipolar RS. The current–voltage (*I*–*V*) characters of the two RS types are illustrated in Fig. 1 [44].

3 Detection of filaments

Although as the most popular model that could be used to explain RS behaviors in many RRAM devices, the filament formation/rupture hypothesis is still under heated debate and controversy. Due to the randomicity of nanoscale filaments arranged in the matrix, clear visualization and characterization of them is very challenging. In order to reveal the underlying RS mechanism, some approaches help to gain insight to these filaments have been developed and will be discussed as follows.

3.1 Resistance–device area relationship

At early stages, several indirect approaches were employed to demonstrate the filamentary working mechanism. One of them is to study the dependence of resistance on electrode area. Figure 2 shows the typical *I*–*V* curves and the relationship between R_{ON}, R_{OFF} and electrode size for the Cu/5%Ce–BFO/Pt cells showing bipolar RS behaviors [45]. The size of the filaments originate from the copper electrode diffusion into the film at LRS is estimated to be dozens of nanometers. As a consequence, most of the current would flow through these nanoscale conductive paths. Due to the much larger electrode area (~ μm^2) than the filament size, the resistance at LRS shows little dependence on the electrode size. However, at HRS, the current is more likely to flow homogeneously through the entire electrode, leading to an increase of resistance with reduced electrode area, as shown in Fig. 2(b). This localized conducting character in the LRS was also demonstrated by Zuo et al. in the Au/ZrO_2: nc-Au/n^+ Si devices through studying the resistive states of two divided devices after cutting the Au electrode of a device at LRS, in which one of them is still at LRS whereas the other one is at HRS [46]. In contrast, the resistances of the Nb-doped $SrTiO_3$ cell at both resistive states are found to be inversely proportional to the cell area [47]. This suggests that the RS in the Nb-doped $SrTiO_3$ is more likely to occur over the whole cell area, which may relate with interface effect, rather than a local region. Thus, characterization of resistance-device area relationship can be employed to

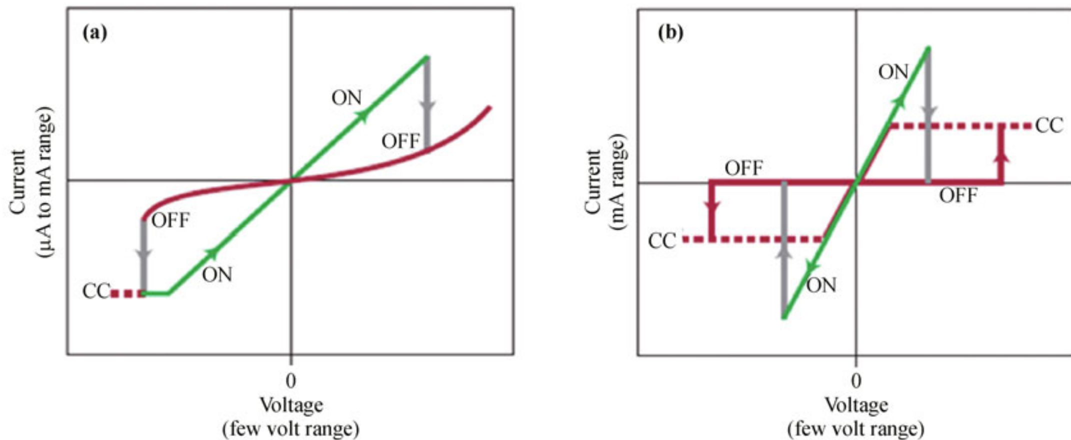

Fig. 1 Typical **(a)** bipolar and **(b)** unipolar RS current–voltage characteristics. (Reproduced with permission from Ref. [44], Copyright 2007 Nature Publishing Group)

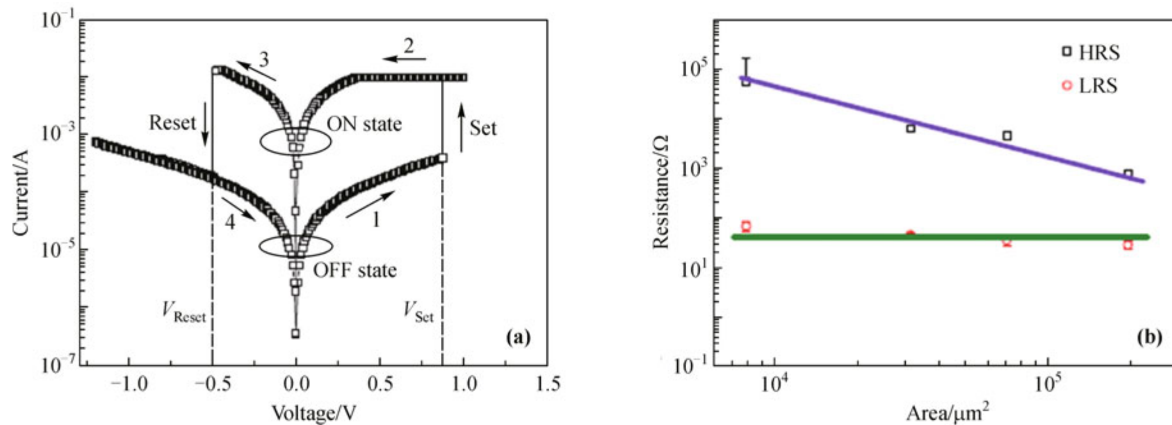

Fig. 2 **(a)** Bipolar RS characteristics of a Cu/Ce–BFO/Pt device. **(b)** Dependence of resistances at different resistive states on the electrode area. (Reproduced with permission from Ref. [45], Copyright 2011 IOP Publishing)

arbitrarily but effectively check whether the filamentary model is applied to the case.

3.2 Resistance–temperature (*R*–*T*) character

As we all know, semiconductors and metals show different *R*–*T* characteristics. The resistance of semiconductors often decreases with increased temperature due to the generation of more thermal induced carriers. On the other hand, the resistance of metals increases with the temperature rise. This is because the increased lattice thermal vibrations at a high temperature can scatter more electrons passing by the lattices and leads to an increment in resistance. The temperature dependence of metallic resistance can be written as $R(T)=R_0[1-\alpha(T-T_0)]$, where R_0 is the resistance at temperature T_0, and α is the temperature coefficient of resistance. In a part of the RRAM memories, the conducting behaviors at HRS and LRS are different from each other. For example, in Ag/5%La–BFO/Pt sandwiched devices whose RS behavior is attributed to metallic Ag filaments formation/rupture, the devices at HRS and LRS exhibit different electrical conducting behaviors with temperature [48]. At ON state, the *R*–*T* curve shows a typical metallic conduction behavior and a semiconductive conduction behavior at OFF state, respectively, as shown in Fig. 3(a) and its inset. The temperature coefficient of resistance of the filaments is calculated to be 2.4×10^{-3} K^{-1}, which is close to the value of 2.5×10^{-3} K^{-1} for high-purity silver nanowires. So it can be deduced that the filaments are composed of metallic silver due to the diffusion of the top electrode under a bias voltage. In Cu/graphene oxide (GO)/Pt device, the device shows a semiconductive conduction behavior and a metallic conduction behavior at HRS and LRS respectively as well [49]. The temperature coefficient of resistance for the filaments is 1.7×10^{-3} K^{-1}, which is smaller than the high-purity copper nanowires (2.5×10^{-3} K^{-1}). It is estimated that some defects like oxygen vacancies are incorporated into the Cu filaments which shorten the mean free path of electrons and reduce the temperature coefficient of resistance [50]. In Ag/La–BFO/Pt device, the devices showing bipolar and unipolar RS behaviors exhibit different temperature coefficients of resistance (Figs. 3(b) and 3(c)). These phenomena imply difference among the conducting filament compositions in the devices.

Superconductors are widely known to show featured *R*–*T* character, where the resistance will drop to zero below a critical superconducting temperature. For example, niobium (Nb) is a superconductor with a bulk superconducting transition temperature T_c around 9.3 K. We fabricated Nb/ZnO/Pt devices showing stable and reproducible bipolar RS behavior, after setting the device to the LRS, the dependence of resistance on the temperature was measured, as shown in Fig. 4. It was found that a sudden drop in resistance at around 7.3 K manifested in the *R*–*T* curve. The slightly different transition temperature from that of bulk Nb can be attributed to the difference in device dimensions and/or the influence of defects [51–52]. After excluding the contribution of Nb electrode to the superconductivity, we can deduce that the Nb elements diffuse into the film and induce the RS.

3.3 Observation by local current atomic force microscopy (LC-AFM)

Another most widely used technology for identifying filaments is to adopt the LC-AFM technique based on scan probe microscopy (SPM) [53]. As a branch of microscopy,

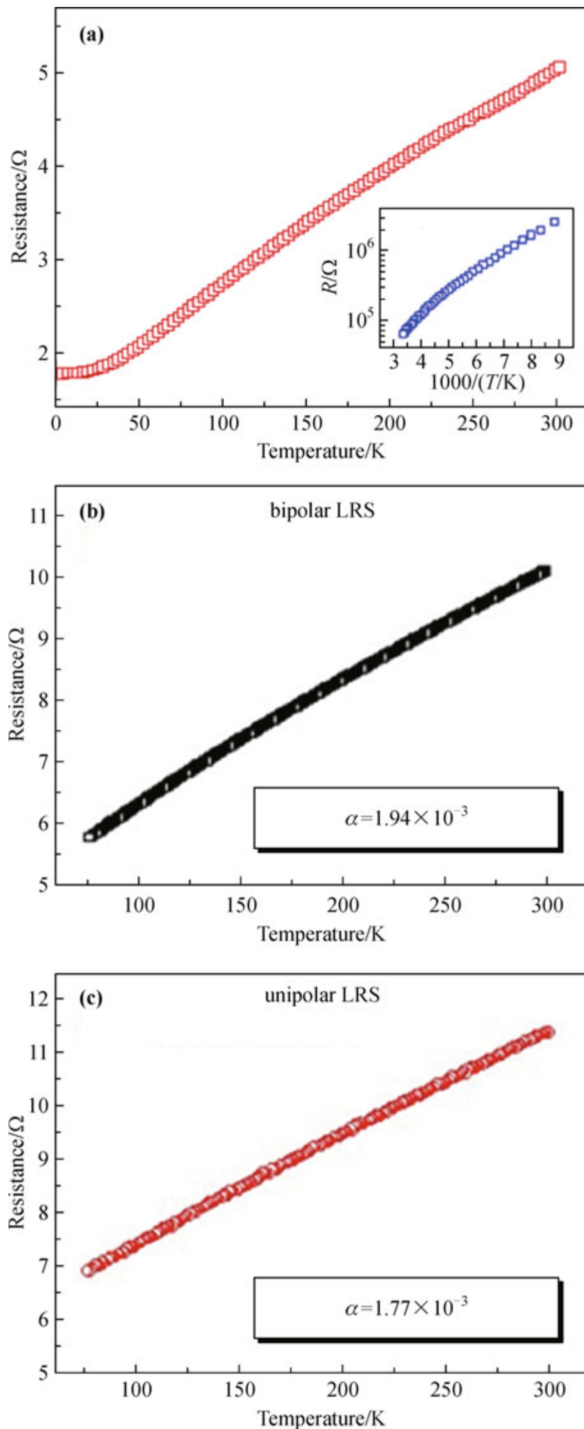

Fig. 3 **(a)** Temperature dependence of resistance of an Ag/La–BFO/Pt memory at LRS. Inset: dependence of resistance on the temperature for the same device at HRS. (Reproduced with permission from Ref. [48], Copyright 2010 IOP Publishing) Temperature dependences of resistance for two Ag/La–BFO/Pt devices at LRS show **(b)** bipolar and **(c)** unipolar RS characteristics. (From Run-Wei Li et al., unpublished results)

SPM can reflect physical properties including morphology, conductivity, magnetism, mechanical information as well as many other properties with a high resolution at nanoscale. After applying a bias voltage between a conductive tip and sample bottom electrode, the tip will scan over the sample surface, and the corresponding current map reflecting electrical properties can be imaged. Local conducting characteristics in various devices have been confirmed by LC-AFM such as BFO [22], TiO_2 [54], ZnO [55] and NiO [24] thin films. For example, Yin et al. reported that in polycrystalline BFO thin film, the RS characters can be directly and clearly illustrated using LC-AFM, as shown in Fig. 5 [22]. A bias voltage of 3 V was first used for current signal detection. For a fresh sample, no obvious leakage current is detected (Fig. 5(a)). With an increase of the bias voltage to 10 V, the leakage current density increases, and more bright regions appear, suggesting the good-conducting character. With a close look at these conducting locations, we can find that the boundaries of the BFO grains appear to be more conductive than the grains (Fig. 5(f)). This implies that these grain boundaries serve as conducting paths for current flow and are more likely the places where the RS happens. Enhanced local conductivity was observed from the current map at a 3 V reading voltage after the 10 V write process (Fig. 5(c)). As a −5 V bias voltage was applied, these conductive regions vanished. These results clearly suggest the writable/erasable (RS) property of the BFO films. Apart from the LC-AFM, other technologies based on SPM such as electrostatic force microscopy (EFM) and Kelvin probe microscopy (KPM) also extend our understanding of the working mechanism as well, which has been recently been reviewed by Lee et al. [56]. However, this technology could only provide the surface information but no details about the structure and composition of the filaments embedded in the film.

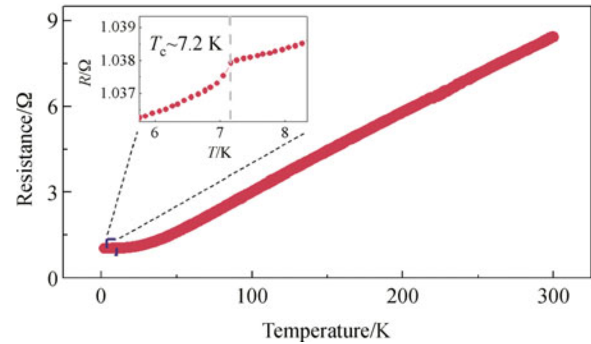

Fig. 4 Temperature dependence of an Nb/ZnO/Pt device resistance at LRS. Inset: zoomed-in curve showing a temperature range from 5.5 to 8.5 K. (From Run-Wei Li et al., unpublished results)

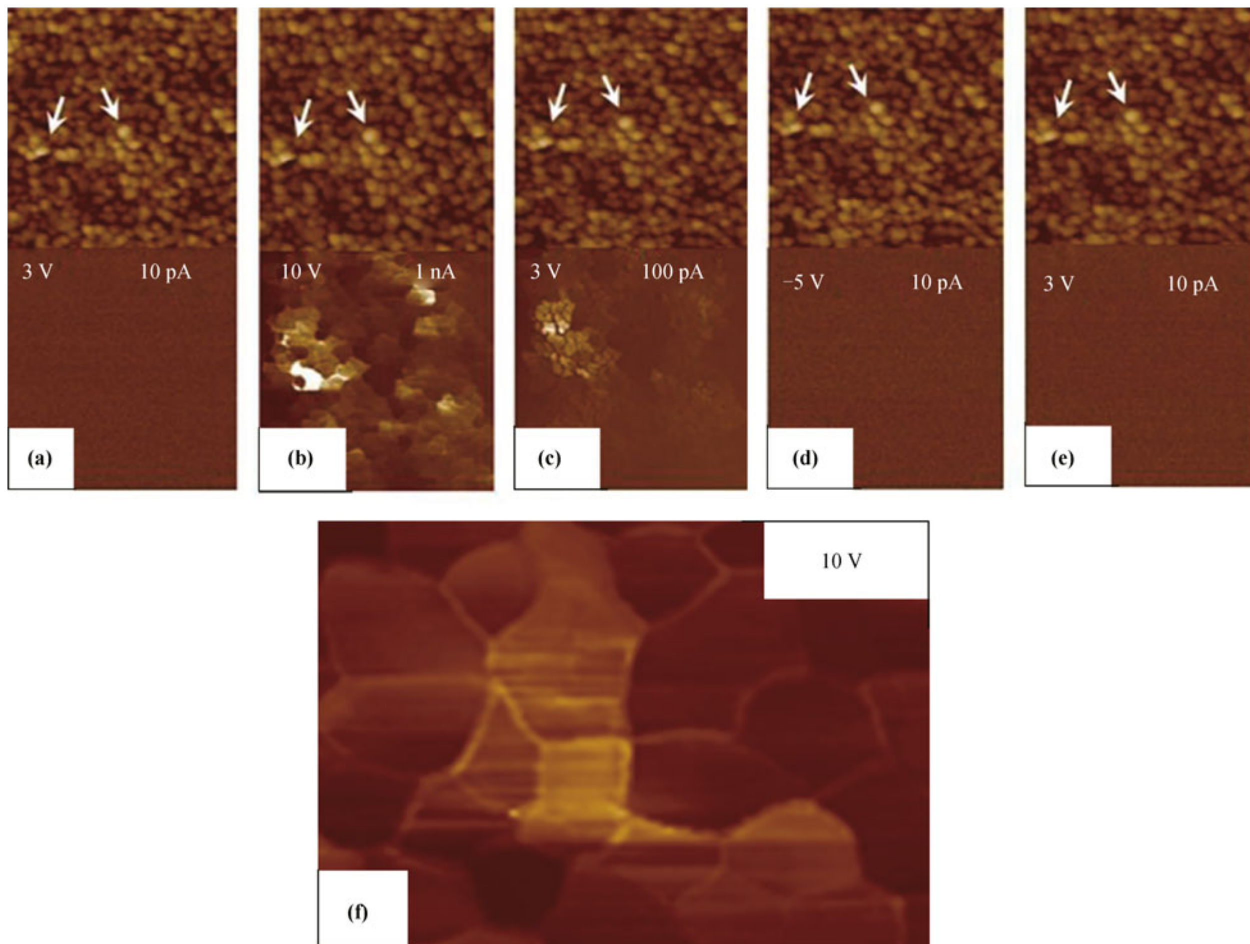

Fig. 5 **(a)(b)(c)(d)(e)** Morphologies and corresponding current maps of BFO film at various bias voltages. **(f)** Local magnified current map of BFO film at a bias voltage of 10 V. (Reproduced with permission from Ref. [22], Copyright 2010 American Institute of Physics)

3.4 Transmission electron microscopy (TEM) characterization

On the way to comprehensively characterize the filaments, TEM plays a very important role in deepening our understanding of these local conducting paths. High resolution TEM images supply visible filament pictures, and yet energy dispersive X-ray (EDX) spectroscopy and electron energy-loss spectroscopy (EELS) measurements can be further applied to confirm the composition of the filaments, which help directly to reveal the intrinsic working mechanism. Some researchers have published their works about detection of filaments using these techniques [57–60]. In Ag/Mn:ZnO/Pt system, Yang et al. inspected the existence of Ag filaments via TEM observation [59]. As shown in Fig. 6 [59], the protrusion-like regions connecting the two-terminal electrodes were observed in a device at LRS. The bridges show cylindrical and inclined conical sharps with size around dozens of nanometers. By performing high-resolution EDX measurement, they confirmed that these filaments are mainly composed of Ag element. Sakamoto et al. also successfully detected a Cu filament embedded in a Cu/Ta_2O_5/Pt resistive switching device after turning the cell on [61]. Thanks to the TEM characterization method, RS originates from the top electrochemically active electrode diffusion becomes more convincing. In addition to the electrode effect, phase change due to non-stoichiometric that induces RS has also been demonstrated. Park et al. clarified that the physical origin of RS phenomenon in NiO_{1+x} film is the formation of Ni filaments that dominate the switching process, supported by the EELS analysis, as shown in Fig. 7 [62]. Si nanocrystals that align in a path parallel to the direction of the electrical field that result in the RS has also being observed in SiO_x film [60].

Instead of detecting the existence of filaments in an RS specimen at LRS, *in situ* TEM allows the investigation of microstructure changes and real time resistance switching

Fig. 6 **(a)** Observation of filaments in an Ag/ZnO:Mn/Pt cell at LRS from cross-sectional TEM image. **(b)** Enlarged part of the square region. **(c)** TEM image with a red line along a filament and corresponding EDX analysis result along the line. (Reproduced with permission from Ref. [59], Copyright 2009 American Chemical Society)

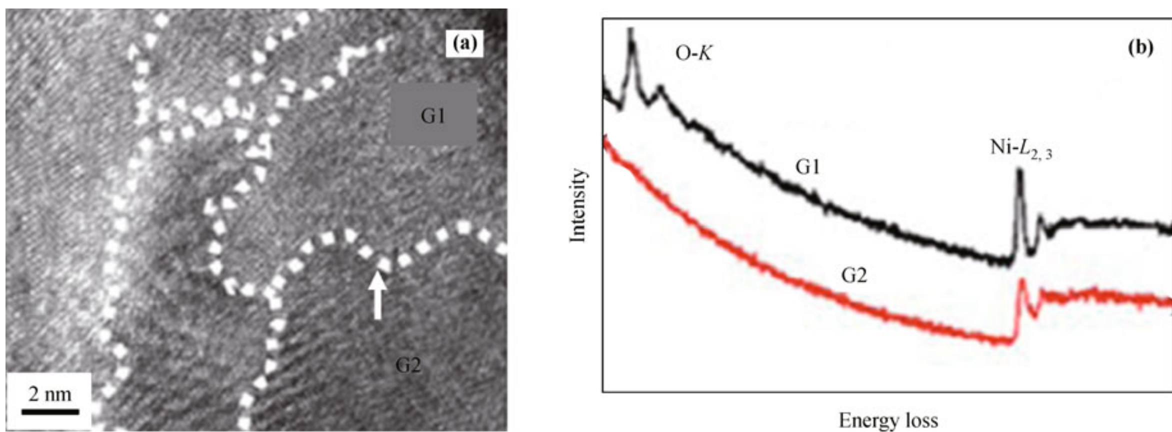

Fig. 7 **(a)** High-resolution transmission electron microscopy (HRTEM) image of the NiO_x film with broken grains indicated by the white dotted lines. **(b)** Corresponding EELS results of the grain (G1) and grain boundary (G2). (Reproduced with permission from Ref. [62], Copyright 2007 American Institute of Physics)

in a fixed region at the same time, which provides more convincing evidences. Direct characterization of the filaments under different bias voltages in Cu/Cu–GeTe/Pt memory has been reported by Choi et al. [57]. Figure 8 illustrates the cross-sectional scanning transmission electron microscopy (STEM) results [57]. At zero voltage, dark regions composed of Cu element were observed in the film due to the existence of dopant Cu in the film. It is clearly seen that these Cu clusters near the Pt tip did not connect the top and bottom electrode. After applying a 0.4 V bias voltage on the Cu electrode relative to the Pt tip, the Cu clusters vertically elongated and finally bridged the two-terminal electrodes, which turn the memory on. Under reversed bias voltages, the filaments were annihilated, and turned the memory off. What's more, multiple filaments growth was also confirmed. These *in situ* STEM results clearly illustrate the evolution of filaments that contribute to the whole RS behaviors.

Based on electrochemical metallization (ECM) theory [31], in resistive switching memories with active electrodes (Ag or Cu) as anode and inert electrodes (Pt) as cathode, when a positive bias voltage is applied on the anode, metal atoms will be oxidized to active metal ions at the anode and migrate to the inert cathode, and eventually reduced back to metal atoms at the cathode/electrolyte interface. With the accumulation of these metal atoms, they will grow toward the anode, and connect the anode with the cathode, eventually turn the memory on. In addition, the filaments are expected to show a shape with a wide base near the cathode/electrolyte interface and a narrow neck near the anode/electrolyte interface, the dissolution of filaments during Reset process should happen from the anode. This

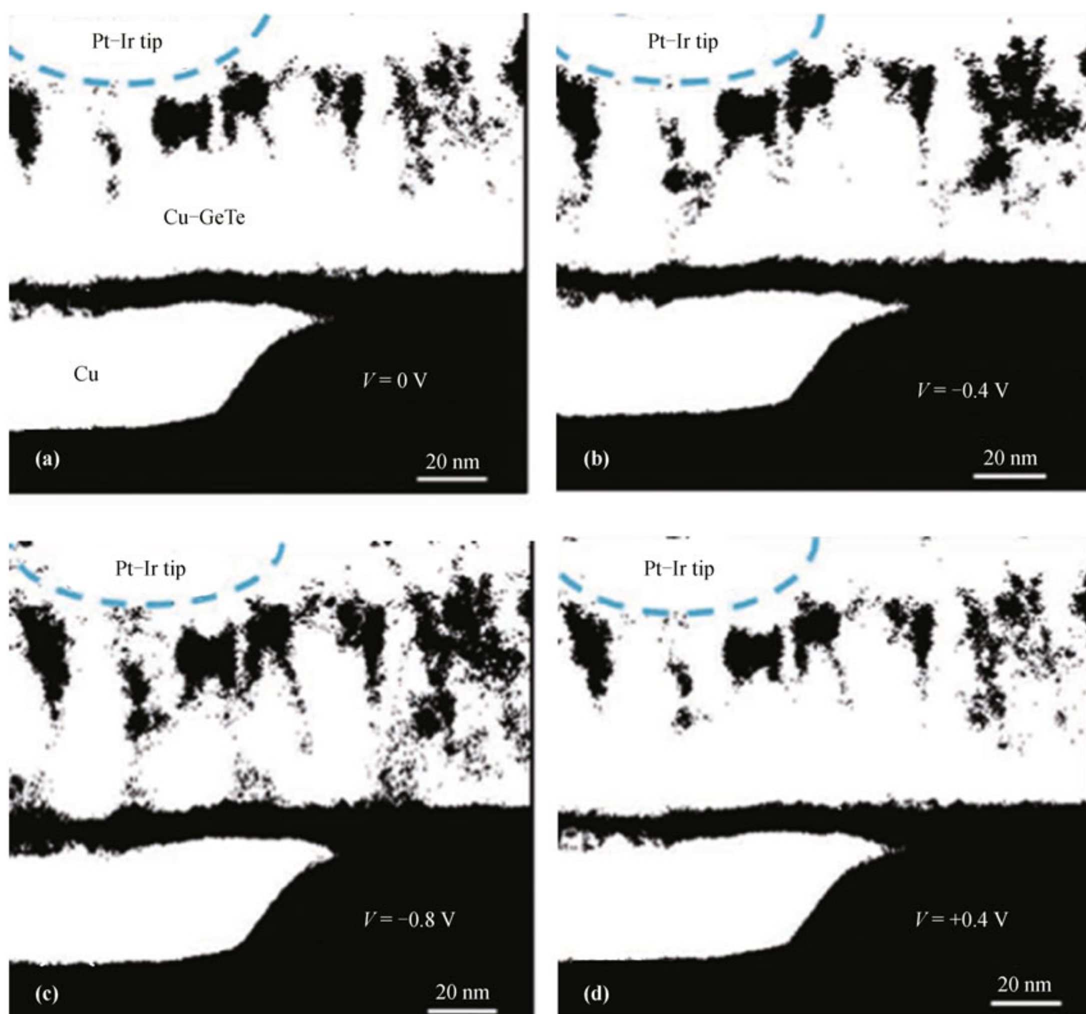

Fig. 8 *In situ* STEM measurements of microstructure changes in a Pt/Cu–GeTe/Cu device after applications of **(a)** 0 V, **(b)** –0.4 V, **(c)** –0.8 V and **(d)** 0.4 V bias voltages on the Pt electrode. (Reproduced with permission from Ref. [57], Copyright 2011 WILEY-VCH Verlag GmbH & Co. KGaA, Weinheim)

hypothesis is widely accepted and has been used to explain many resistive switching mechanisms in various devices [57,63–65]. Although it has been verified experimentally in chalcogenide-based electrolyte system, whether it is also applicable to oxide-based electrolyte system has never been clear addressed. Liu et al. recently clarified this issue by *in situ* real time observing the filaments formation/dissolution process in oxide-electrolyte-based resistive switching memories [66]. In the Ag/ZrO_2/Pt device, after Set process, they observed that the Ag filament exhibits a shape with a ~30 nm base near the Ag electrode and a ~5 nm narrow point near the Pt electrode (Fig. 9(a)), which contradicts to the widely accepted ECM theory. In addition, during the filament dissolution process in Cu/ZrO_2/Pt device, they also found that the filament began to dissolve from the cathode where the narrowest part of filament exists toward the anode, eventually, leaving a part of filament insoluble attached to the anode (see Figs. 9(b) and 9(c)), rather from the anode. These phenomena have also been demonstrated by Yang et al. in SiO_2-based resistive memories (Fig. 9(d)) [67]. In fact, the dynamics of filaments growth and dissolution are closely related to the metal ions transport behaviors in the switching media. For chalcogenide-based electrolyte materials such as Ag_2S and CuGeS with high solubilities and diffusion coefficients of metal ions like Ag^+ and Cu^{2+}, these metal ions can only get enough electrons to reduce back to neutral metal atoms at cathode. However, for oxide-electrolyte like ZrO_2 with much lower solubility and diffusion coefficients of metal ions, during metal ions migration process under electrical fields, the device conductivity is mainly contributed by electron transport. Thus, these metal ions can easily capture electrons then reduce back to atoms in the electrolyte, leading to the growth of filament from anode to cathode, and form filament with the narrowest part connecting the cathode (Fig. 9(d)). So it is reasonable to expect that during the Reset process, the filament will dissolve from the cathode first. In addition from the oxide-electrolyte, Yang et al. also observed a different filament growth mode in a-Si based resistive memories by employing *in situ* TEM characterization method [67]. Instead of forming a solid continuous Ag nanowire, the conductive path is composed of a chain of nanoparticles separated by nanogaps, where the electrons can tunnel between these nanoparticles and contribute to the conductivity of the device. This observation further demonstrated that the Ag cations can capture electrons in the electrolyte without reaching the cathode, which is different from that in chalcogenide-based ECM cells.

Apart from the *in situ* observation, Peng et al. also successfully demonstrated that the concial shaped filaments rupture position in oxide-based electrochemical metallization memory cells is near the cathode place from another perspective [68]. Based on the opinion that Cu ions diffuse into the ZnO film and form Cu filaments, they found that the *I–V* characteristics of the Cu/ZnO/Pt and Cu/ZnO/(Al:ZnO) devices at the HRS are different as shown in Fig. 10 [68]. By analyzing the dependence of the *I–V* characteristics with the Schottky barrier heights induced by the Cu filaments and electrodes, they concluded that the filaments should have a concial sharp and rupture at the weakest position near the cathodic interface, in consistence with the results obtained by Liu et al. and Yang et al.

Characterizing the evolution and properties of the filaments not only help us comprehensively understand the RS behavior, but also provide guidelines to the device design and obtain desirable RRAMs.

4 RS performances enhancement

As aforementioned, one of the basic requirements in memories for practical applications is the stability and reproducibility. For the filament model based RRAMs, according to the random circuit breaker (RCB) network model proposed by Chae et al. [54], the distribution of filaments in the switching matrix is generally random. This leads to a large variation of switching voltages for different cells from time to time. The local conducting paths at nanoscale make it difficult to manipulate the formation/rupture of filaments artificially, as a consequence, makes it hard to achieve stable and reproducible RS characteristics. Thus, how to control the filaments is an open question. In order to improve the RS stability and reproducibility, some approaches have been employed and turned out to be effective.

4.1 Electrode effects on RS performances

As an important part in the “MIM” structure, electrodes definitely play a very important role in affecting the memory performances. In general, the effect of electrodes on RS can be classified into two categories: first, the electrochemically active electrode atoms diffuse into the switch matrix under an electrical field and result in the RS behavior, and second, the electrode-film interface effect. In metal/La–BFO/Pt memory devices, cells with different top metal electrodes such as Al, Ag, Cu and Au were found to

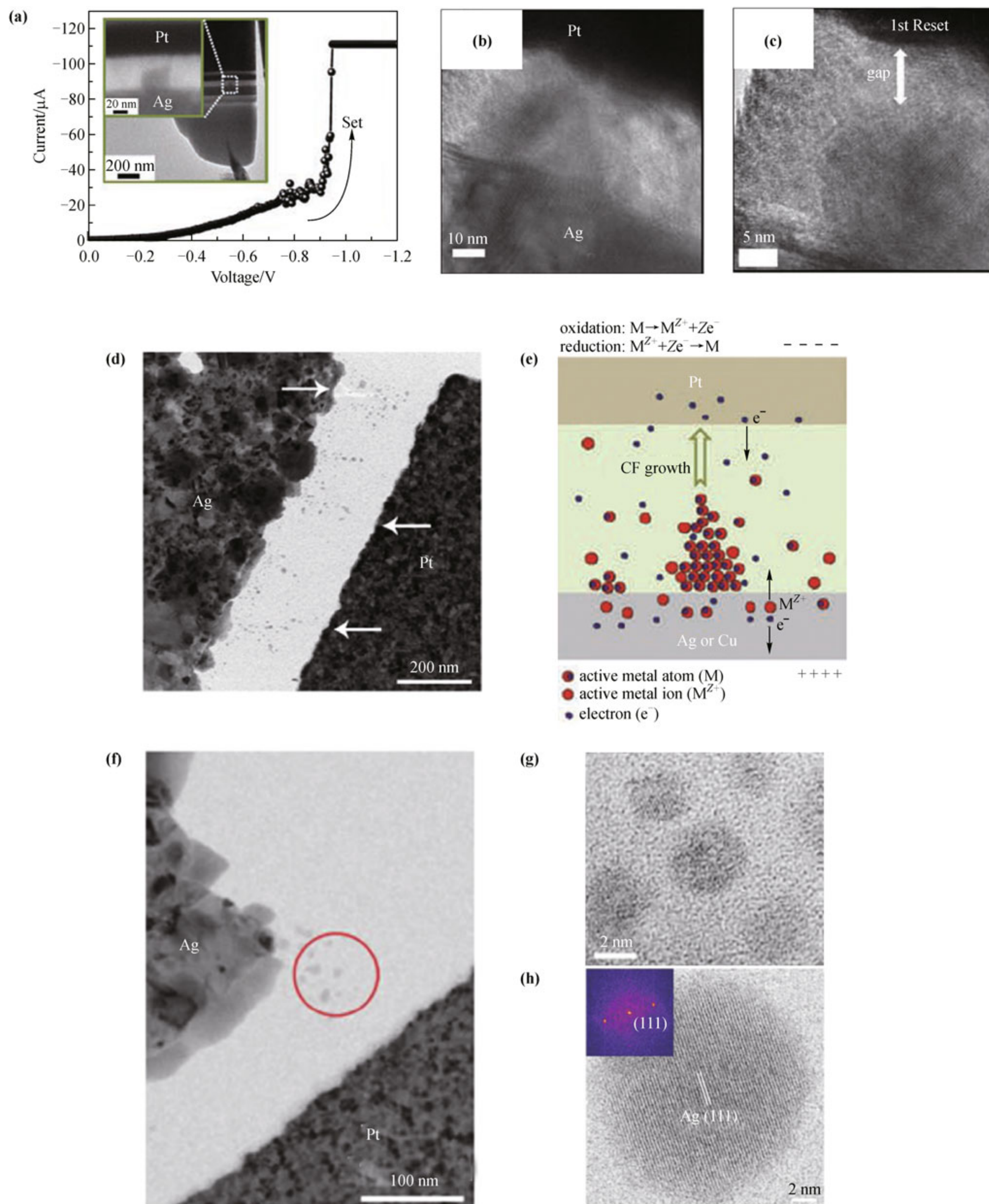

Fig. 9 **(a)** *I*–*V* curve of the $Ag/ZrO_2/Pt$ device during Set process. Inset: TEM image of the device after Set process. TEM images of a filament in a device after **(b)** Set process and **(c)** Reset process. **(d)** TEM image of the $Ag/SiO_2/Pt$ device after Reset process. **(e)** Schematic of filament growth mechanism. **(f)** TEM image of the Ag/a-Si/Pt device after Reset process. **(g)** HRTEM image of the Ag nanoparticles inside the filament. **(h)** Bright-field STEM image of the Ag nanoparticle. Inset: corresponding fast Fourier transformation results of the HRTEM image. ((a)(b)(c)(e): Reproduced with permission from Ref. [66], Copyright 2012 WILEY-VCH Verlag GmbH & Co. KGaA, Weinheim; (d)(f)(g)(h): Reproduced with permission from Ref. [67], Copyright 2012 Nature Publishing Group)

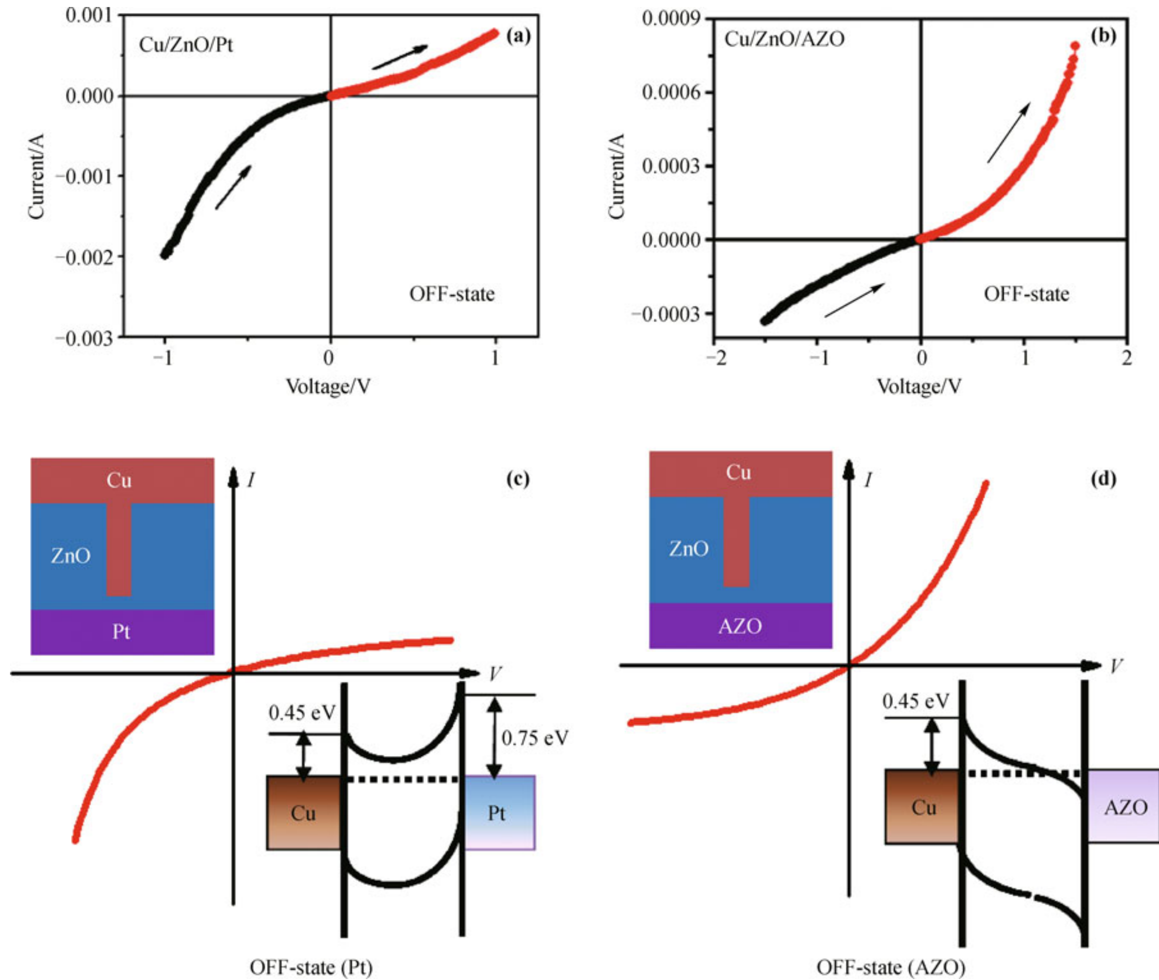

Fig. 10 Typical *I*–*V* characteristics of **(a)** Cu/ZnO/Pt and **(b)** Cu/ZnO/AZO ECM cells at OFF-state. Schematic ideal *I*–*V* characteristics of possible OFF-states of the **(c)** Cu/ZnO/Pt and **(d)** Cu/ZnO/AZO ECM cells. The insets schematically illustrate the possible OFF-states of the cells and the corresponding band diagrams of the insulating gaps (i.e., ZnO) sandwiched between Cu filament and Pt or AZO electrode. (Reproduced with permission from Ref. [68], Copyright 2012 American Institute of Physics)

exhibit different RS properties [48]. The devices with electrochemically active Ag and Cu metals as top electrodes are much more stable compared to the Au, and Al cases showing larger variations in switching voltages, as shown in Fig. 11 [48]. Due to the diversity of the electrode work function, the dependence of the RS behaviors on the work function can be ruled out. It has been demonstrated that Ag and Cu atoms can be easily oxidized to metal ions under a sufficiently high electrical field and diffuse into the films. For the device with Au electrode appears to be less stable and can be ascribed to the much large ionic radius of Au atom as well as gold's chemical inertness which makes it hard to diffuse into the film. For Al electrode, it is most likely that a thin AlO_x layer was formed between the Al electrode and the film. The switching mechanism mainly related with the interface, involving the trap/detrap of carriers.

In metal/GO/Pt structured sandwiches prepared by Zhuge et al. [49], whose RS behaviors are closely related to the electrodes, the Ag/GO/Pt structured device has the highest device yield and lowest Forming voltage (Fig. 12). It is said that a larger ion diffusion coefficient of Ag element compare to other metal elements leads to the low switching voltage, thus even Forming process free, which favors the practical application. The dependences of switching voltages, resistances as well as device yield on electrode imply the importance of electrode plays in the RS behaviors, and may provide guidelines for devices electrode material selection.

In addition to the top electrode (or anode) effects on the RS performances, appropriate design on bottom electrode (or cathode) structure can also be used to improve the RS behaviors. As discussed above, filaments grow from the electrochemically active anode toward the inert cathode

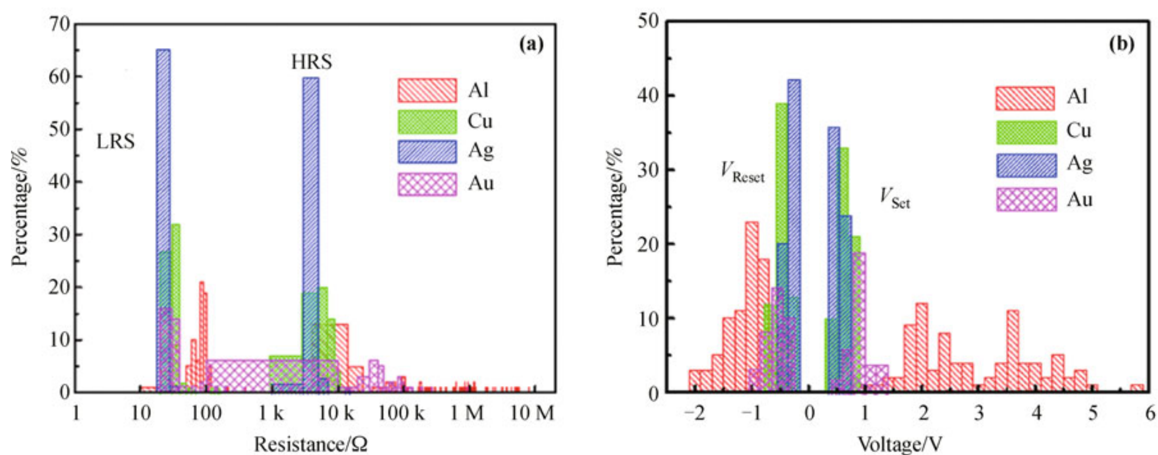

Fig. 11 Statistical distribution of **(a)** resistances in different resistive states and **(b)** switching voltages of the metal/La–BFO/Pt sandwiches with Al, Cu, Ag, and Au as top electrodes. (Reproduced with permission from Ref. [48], Copyright 2010 IOP Publishing)

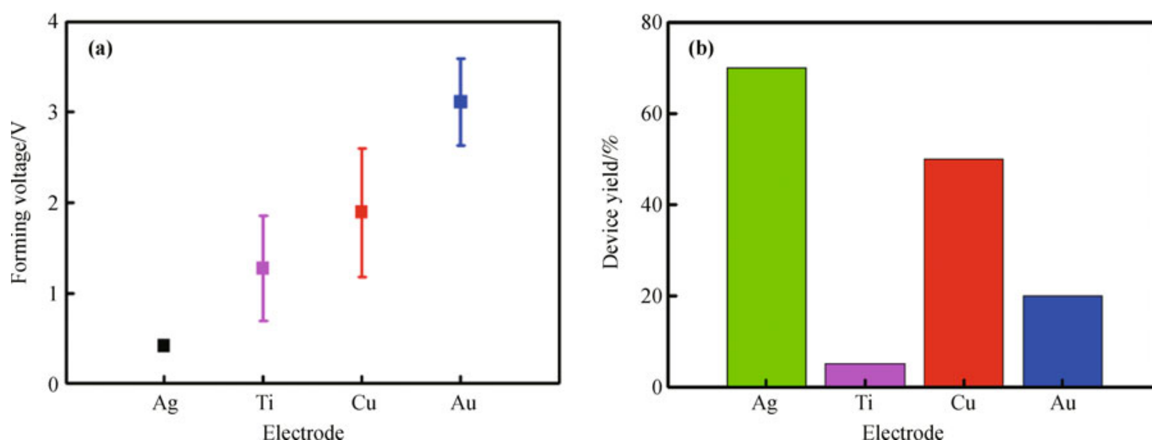

Fig. 12 **(a)** Forming voltages and **(b)** device yields of the metal/GO/Pt devices with Ag, Ti, Cu, and Au as top electrodes. (Reproduced with permission from Ref. [49], Copyright 2011 Elsevier)

along the electrical field direction in some RS sandwiches like Ag/ZrO_2/Pt. However, due to the uniform distributed electrical fields in the switching matrix, the location of filament is always random, which makes it hard to achieve stable RS devices. Liu et al. designed an approach to resolve this challenge by pre-depositing some metal nanocrystals as the bottom electrode on the plane conductive substrate (Fig. 13) [69]. Because of the nanocrystals electrodes protuberated from the substrate, the electrical field distribution around these nanocrystal clusters is enhanced. It is calculated that the magnitude of electrical field near these copper crystals is 2–3 times larger compared to the plane conductive substrate. Thus, more metal ions are expected to accumulate around these metal islands, and the filament location could be considerably controlled. To verify this exception, they performed TEM measurement to capture the filaments formation position. Figure 13(c) shows the cross-sectional TEM image of a specimen after Set process. A nano-bridge connecting the top Ag electrode and bottom Cu nanocrystals has been confirmed. Furthermore, this composition of the bridge made of Cu was also identified by EDX measurement. So it can be concluded that these nanocrystals successfully confined the filaments formation positions. *I–V* measurement suggests stable and uniform RS cycles with narrow distribution of switching voltages. The devices with the nanocrystal clusters exhibit excellent stability in switching voltages. So, devices with suitable nanocrystal clusters array could be further designed and may be useful to achieve more stable RRAM devices.

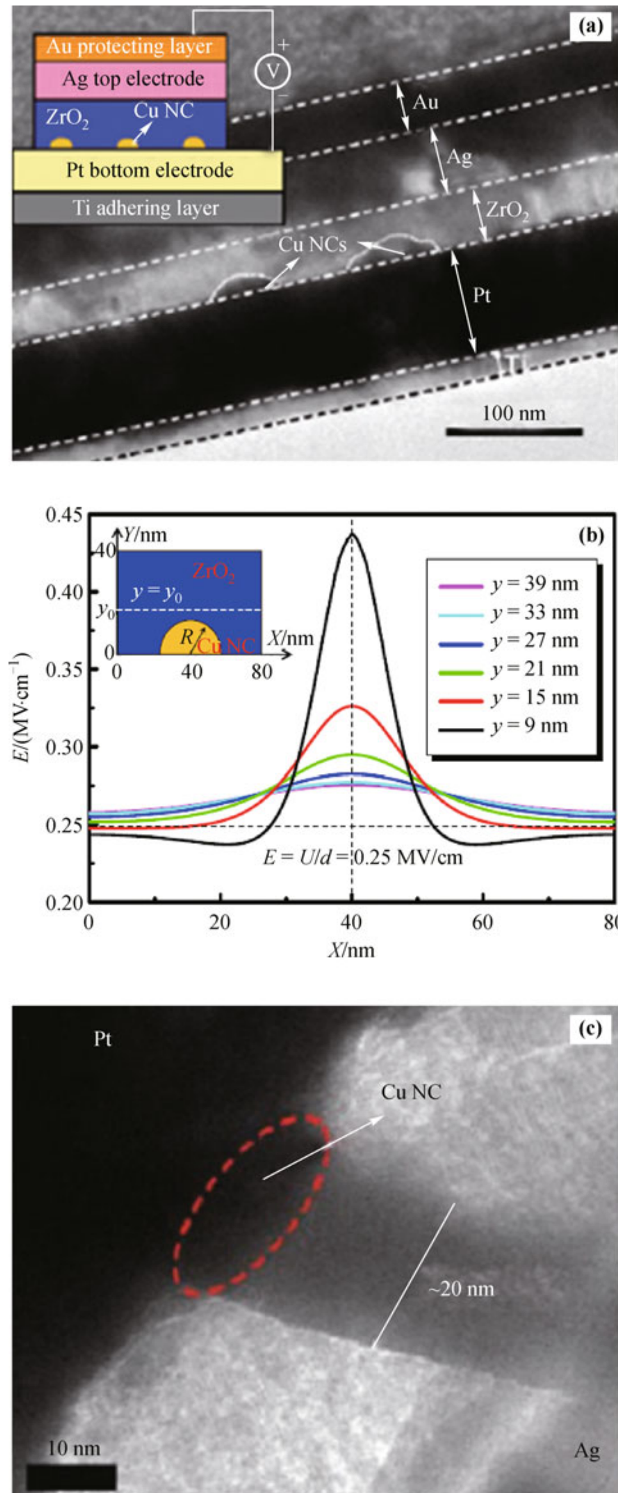

Fig. 13 **(a)** Cross-sectional TEM images of an Ag/ZrO_2/Pt device with Cu nanocrystals covered on the bottom electrode. **(b)** Simulations of the distribution of electrical field around a metal nanocrystal with different radiuses. **(c)** Observation of the formation of filaments that connect the Cu nanocrystal and the Ag electrode. (Reproduced with permission from Ref. [69], Copyright 2010 American Chemical Society)

4.2 Microstructure dependence of RS behaviors

4.2.1 Crystallization effect

The microstructure of the switching matrix can also affect the performances of the RS memory drastically. According to Lee et al., defects in crystalline materials tend to accumulate around the grain boundaries and dislocations [12]. External or intrinsic defects such as active electrode ions in RRAM devices can easily bond to these extended structures [70–71]. In amorphous oxide films, where extensive oxygen vacancies or the injected foreign active electrode ions were homogenously distributed, the positions for the formation of filaments are random as well as the growth direction. As a result, the shape of the filaments is always like a tree with many branches, as evident from the optical microscope image in Ag/H_2O/Pt device, which in further leads to the large variation in the switching voltages [65].

Compared to the amorphous films, the crystallized films seem to exhibit better performances in stability. In single crystalline $SrTiO_3$, it has been demonstrated that the places where RS happens are confined by the dislocations [25]. For polycrystalline BFO films, the film crystallinity is strongly dependent on the fabrication methods, i.e. the annealing temperature [22,72]. The BFO grain size increases and grain boundaries density decreases respectively with an increase of annealing temperature, as shown in Figs. 14(a)–14(c). Electrochemically active metal ions like Cu^{2+} from the top electrode are expected to diffuse into the film along the grain boundaries under an applied electrical field. From the RS *I*–*V* curves for Cu/BFO/Pt cells with different film crystallinity as shown in Figs. 14(d)–14(f), it is found that with the increase of crystallinity (decrease of grain boundary density), the resistances and switching voltages become much more stable. According to Zhuge et al. [55], conducting channels tend to locate at the grain boundaries in polycrystalline ZnO film have been demonstrated by employing LC-AFM technology, as shown in Fig. 15. Thus, the improved stability of the BFO devices can be understood that in crystallized BFO films the location and growth direction of the filaments were confined by the grain boundaries, which eventually results in a much smaller variation in switching voltages.

4.2.2 Oxygen content in oxides

In memories whose RS performances are dominated by the electrodes, the switching matrix usually just serves as the

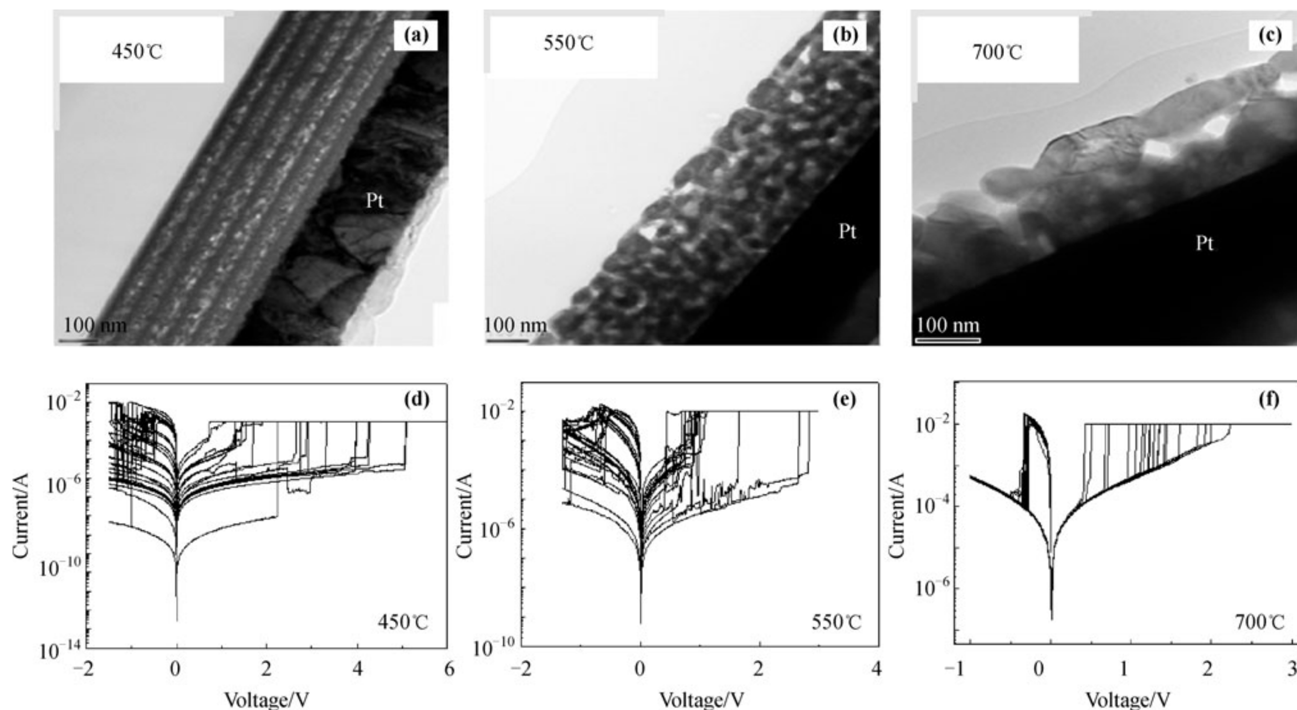

Fig. 14 Cross-sectional TEM images of BFO films annealed at **(a)** 450°C, **(b)** 550°C, and **(c)** 700°C. (Reproduced with permission from Ref. [22], Copyright 2010 American Institute of Physics) Current–voltage characteristics of BFO films annealed at **(d)** 450°C, **(e)** 550°C, and **(f)** 700°C. (From Run-Wei Li et al., unpublished results)

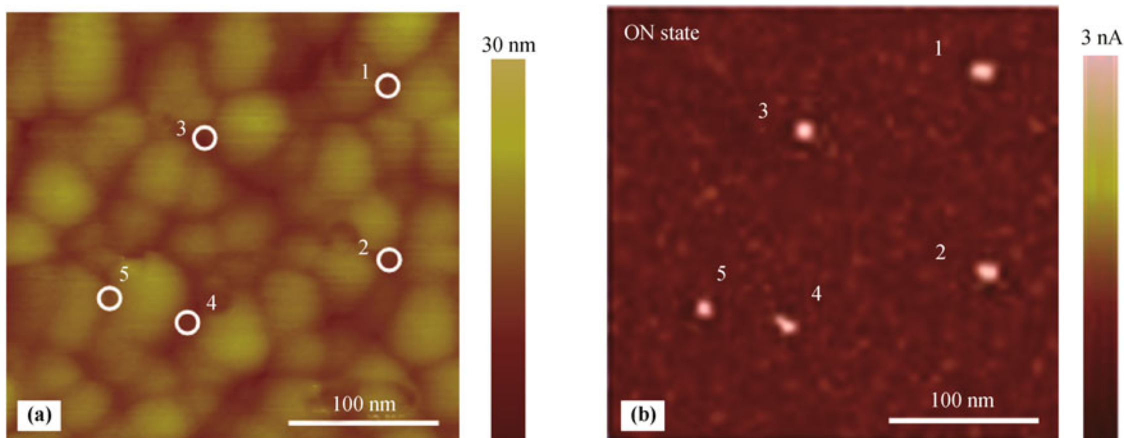

Fig. 15 **(a)** Morphology and **(b)** corresponding current map of ZnO deposited at room temperature (RT) in the ON state under a read voltage of 1 V. (Reproduced with permission from Ref. [55], Copyright 2011 IOP Publishing)

conducting media for ions/electrons transportation. However, for some other RRAMs, the switching mechanism is closely related with the properties of the dielectric layer, especially in oxide films. The RS performances of oxide films are sensitive to the oxygen vacancies concentration, which could be modulated during the film fabrication process. For instance, Park et al. found that in NiO_x film deposition process, the oxygen content in the sputtering gas mixture seriously influence the electrical conductivity of the films, as illustrated in Fig. 16 [73]. For samples deposited in a mixture with 5% oxygen content, the film is highly conductive, and no RS can be observed. With an increase of oxygen content from 5% to 20%, the unipolar RS behavior shows up gradually but turns to threshold switching type finally. These phenomena can be understood by the variation of defects content such as Ni vacancies and oxygen vacancies. Similar phenomenon has also been reported by Bae et al. in TiO_{2-x} film deposition

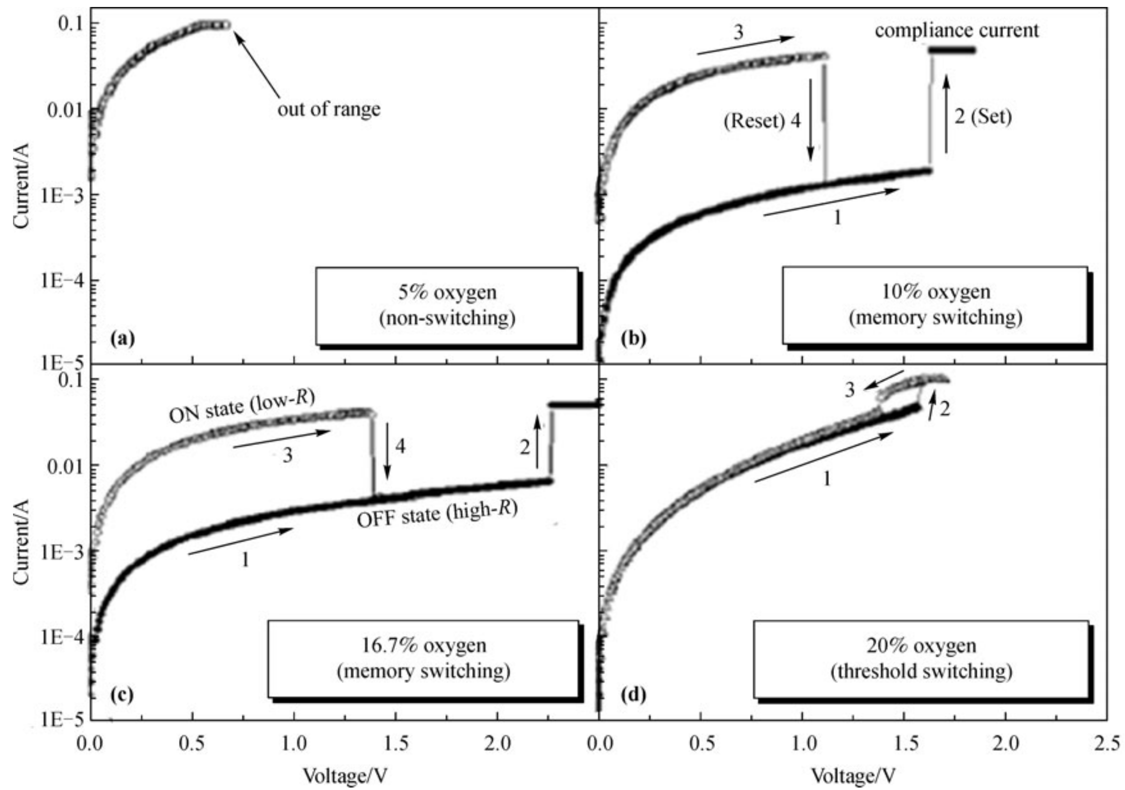

Fig. 16 Current–voltage characteristics of the Pt/NiO/Pt devices with NiO films fabricated at different oxygen contents: **(a)** 5%; **(b)** 10%; **(c)** 16.7%; **(d)** 20%. (Reproduced with permission from Ref. [73], Copyright 2006 American Vacuum Society)

process [74]. These results suggest that the deposition condition for films fabrication also plays an important role in affecting the RS behavior drastically.

4.2.3 Doping effect

Doping is reported to be useful in improving the performances of RS behaviors. By first principles calculation, Zhang et al. found that trivalent dopants Gd can decrease the oxygen vacancy formation energy of the HfO_2 film [75]. Compared to the random formation positions of oxygen vacancies in undoped film, these defects can be easily generated near the dopants in the doped films and help to stabilize the oxygen vacancies filaments, and suppress the randomicity of switching voltages and resistive states, as shown in Fig. 17 by the

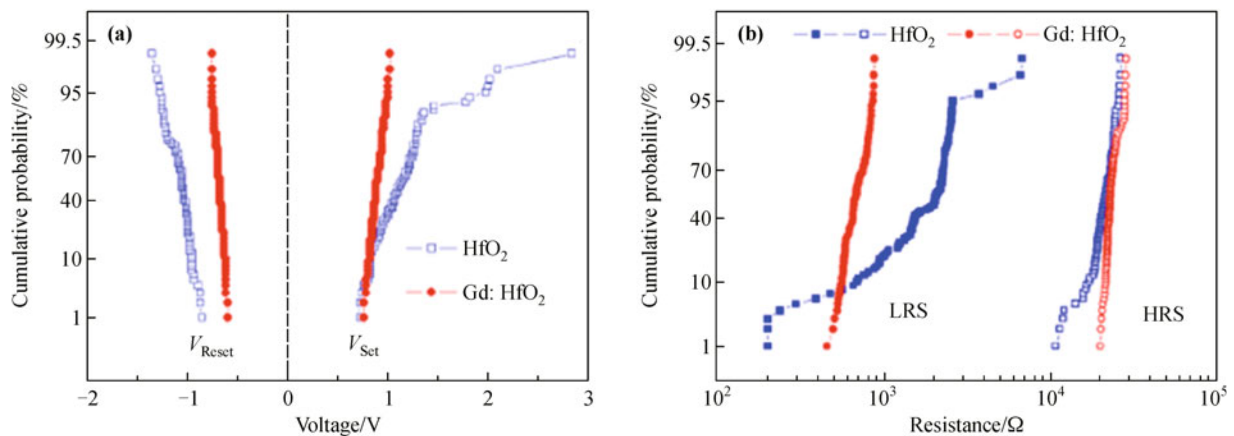

Fig. 17 Measurements of **(a)** switching voltage distribution and **(b)** resistance distribution in different resistive states for TiN/Gd–HfO_2/Pt and TiN/HfO_2/Pt devices. (Reproduced with permission from Ref. [75], Copyright 2011 American Institute of Physics)

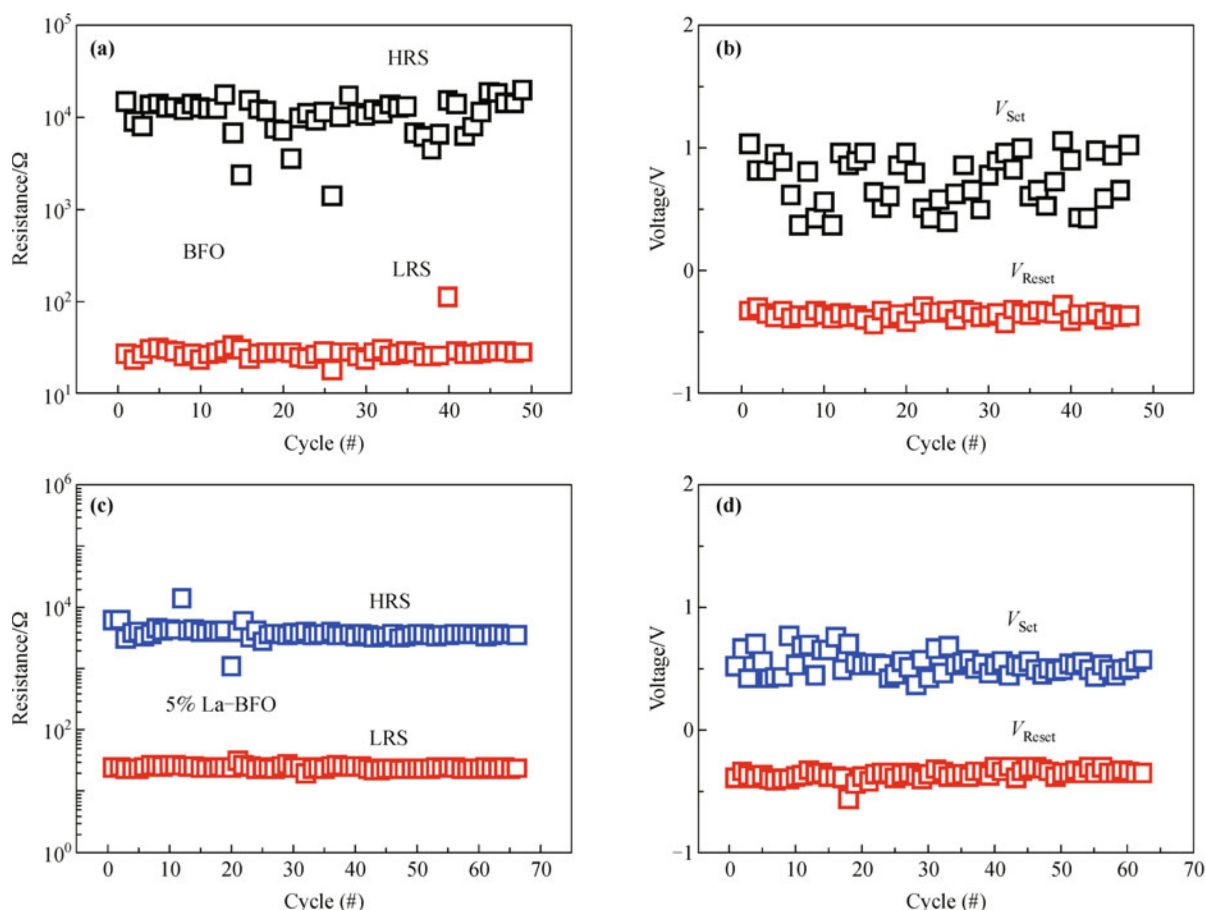

Fig. 18 Statistical distributions of resistances in HRS, LRS and switching voltages of **(a)(b)** Cu/BFO/Pt devices and **(c)(d)** Cu/5%La–BFO/Pt devices. (From Run-Wei Li et al., unpublished results)

resistances and switching voltages distributions [75]. We also obtained similar results in undoped and 5% La doped BFO films annealed at 700°C as shown in Fig. 18.

In Cu/ZrO_2/Pt devices, the improvement on RS performances has also been achieved by tetravalent Ti doping [76]. The Forming process for initiating the device RS property is eliminated. Furthermore, the reproducibility is enhanced and the variations of switching voltages are also reduced. Liu et al. explained that, after Ti ion implantation, the concentration of defects like oxygen vacancies in the ZrO_2 film is lifted. The defect concentration level required for Forming process is lowered, so the Forming voltage is largely reduced and Forming process is eliminated. These Ti impurities were also considered as the seeds for the formation of the conducting channels, and led to excellent RS performances including the stability of the R_{OFF}. In BFO system, we found that by doping foreign atoms with the same valence but different atom radiuses, the Forming voltages can also be different (Fig. 19). With 5% Ce doping into the film, the Ag/Ce–BFO/Pt devices show much smaller Forming voltage compared to the pure case. This indicates that the RS performances can be modulated by dedicatedly choosing different dopants.

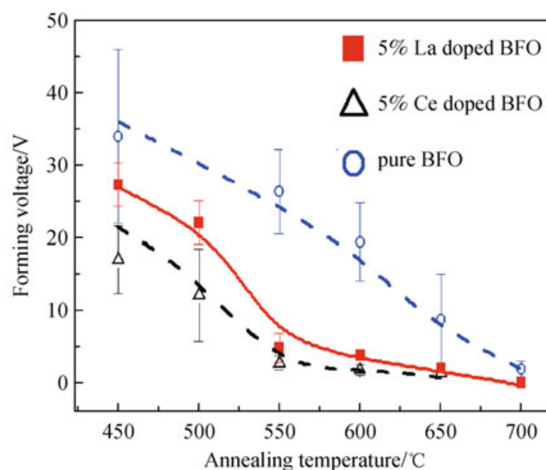

Fig. 19 Dependence of the Forming voltages on annealing temperatures of pure BFO films and doped BFO films sandwiched between Cu and Pt electrodes. (From Run-Wei Li et al., unpublished results)

Suitable introducing foreign elements into the films can decrease the concentration of carriers that improves RS behavior. Zhuge et al. [55] reported that in polycrystalline ZnO films, although the crystallinity can be improved by depositing films at high temperatures, the current density increase as well, which results in a much lower resistivity, thus no RS phenomenon (Fig. 20). By doping N as an acceptor, the electrons induced by the intrinsic defects including oxygen vacancies and zinc interstitial atoms were partially compensated. So the resistivity is lifted, RS behavior could be observed. It is found that the conducting paths are mostly located at the grain boundaries and the doped device with less grain boundary density shows more stable resistive states as well as switching voltages.

In addition to the electrode and microstructure affection, other factors like temperature, atmosphere or even the

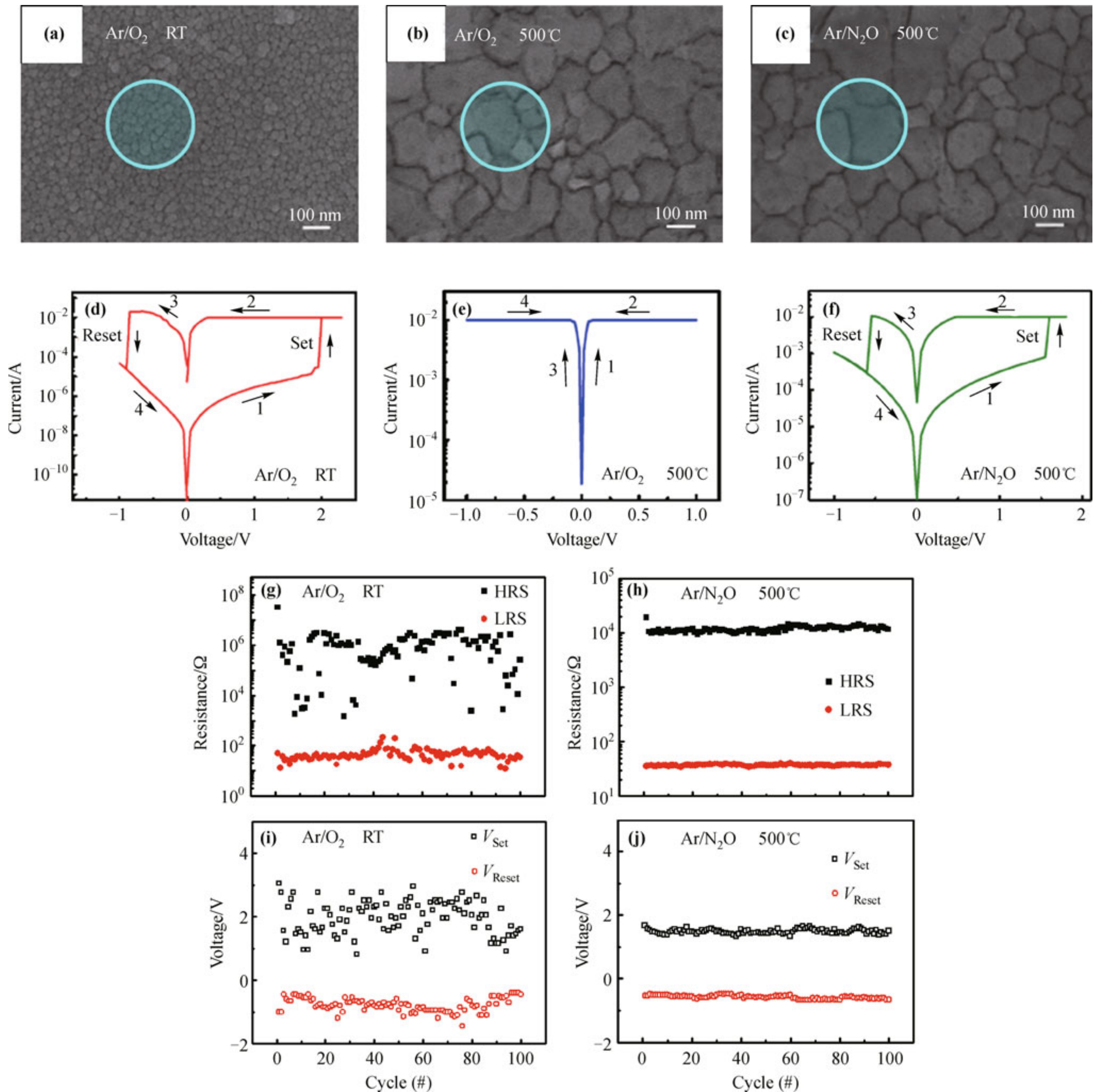

Fig. 20 SEM images of **(a)** ZnO films deposited at RT, **(b)** ZnO films deposited at 500°C, and **(c)** N-doped ZnO films deposited at 500°C. **(d)(e)(f)** Corresponding current–voltage characteristics of the film sandwiched between Cu and Pt electrodes. **(g)(h)(i)(j)** Distributions of resistances and switching voltages for RT deposited ZnO films and N-doped ZnO films deposited at 500°C. (Reproduced with permission from Ref. [55], Copyright 2011 IOP Publishing)

moisture are reported to plays very important roles in influencing the device performances [77–79]. In order to effectively modulate the RS performances, we should comprehensively understand the intrinsic working mechanism and find out the main factors that could affect the switching properties.

5 Quantum conductance behaviors in oxide-based RRAMs

In many RRAMs, the filaments size is usually at nanoscale or even smaller. As these filaments further reduced to atomic scale size, it is natural to expect the quantum size effects, such as quantized conductance. It has already been reported by Terabe et al. that in solid state electrolyte, by changing the size of a Ag construction between Pt and Ag_2S electrodes modified by external electrical pulse, this will lead to the discrete conductance changes in units of quantum conductance [64]. Based on this property, multilevel storage for ultrahigh density memory applications may be achieved. Recently, quantum conductance behaviors in oxide-based RRAMs have also been observed [80].

The Nb/ZnO/Pt devices showing bipolar RS characteristics, whose RS mechanism can be attributed to the diffusion of Nb elements into the device, multiple current jumps were frequently detected in the RS processes. A typical *G*–*V* curve in the Set process was illustrated in Fig. 21(a). *G* represents the electrical conductance calculated as $G = I/V$, where *I* is the current and *V* is the voltage, and *G* was recorded in units of the quantum conductance $G_0 = 2e^2/h$, where *e* is electron charge and *h* is Planck's constant. Abrupt conductance increase followed by a stable conductance plateau can be clearly seen from the curve. For example, the conductance increases suddenly from G_0 to $3G_0$ at 0.8 V followed by a plateau of $4G_0$. Similar behaviors can also be observed at 1.3 and 1.45 V, respectively. Statistics count of the conductance changes from two hundred curves as shown in Fig. 21(b) confirms the quantum conductance behaviors, which demonstrates the formation of discrete quantum channels in the device [81]. These phenomena were also observed in the Reset process. Figure 21(c) shows the relationship between the conductance and the bias voltage for a Nb/ZnO/Pt device in the LRS and the inset is the corresponding *I*–*V* curve in a larger voltage range from 0 to −2 V. Multiple conductance drops and plateaus on the integer multiples values of G_0 corresponding to the rupture of discrete quantum channels can be clarified. In order to demonstrate

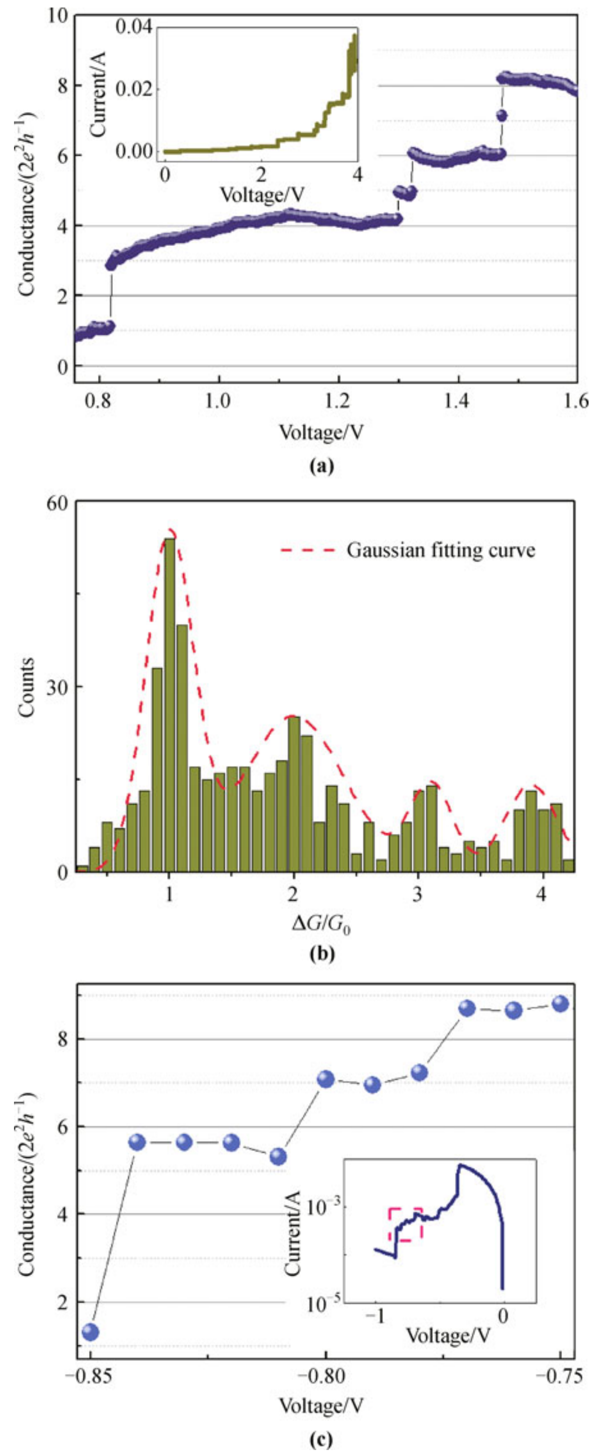

Fig. 21 Resistance switching of Nb/ZnO/Pt junctions: **(a)** Measured conductance as a function of the bias voltage during the Forming process. Inset: corresponding *I*–*V* curve in a larger voltage range from 0 to 4 V. **(b)** Histogram of the conductance changes Δ*G* obtained from the Forming and Set processes. Dotted line: Gaussian fitting curve of the histogram as a guide to the eyes. **(c)** *G*–*V* curve showing apparent quantized conductance behaviors in the Reset process. Inset: corresponding *I*–*V* curve in a larger voltage range from 0 to –2 V. (Reproduced with permission from Ref. [80], Copyright 2012 WILEY-VCH Verlag GmbH & Co. KGaA, Weinheim)

the quantized conductance phenomenon originates from the nature of quantum channels, the ITO/ZnO/ITO devices showing unipolar RS characteristics whose behaviors can be understood based on the formation/thermal rupture of filaments composed of oxygen vacancies were fabricated [82]. Quantum conductance phenomena were also detected, which excluded the dependence of the featured quantum behaviors on the specified devices materials.

Despite of the promising potential being used as ultra-high density memories, further control of the quantum behaviors is very essential and need to be addressed. We found that the discrete quantum conductance is strongly affected by the electrical parameters such as compliance current and bias voltage amplitude. Take the Nb/ZnO/Pt devices as an example, as can be seen in Fig. 22(a), the electrical conductance of the device increases monotonously with the increase of compliance current level. Initially, the device shows a stable conductance of $2.5G_0$, where the half integer quantum conductance values may originate from the adsorbed impurities on or in the atom chains [83–84]. With the increase of compliance current level from 2.5×10^{-4} to 4.0×10^{-4} A in steps, the electrical conductance was switched from $2.5G_0$ to $8.5G_0$. On the other hand, the conductance value can be modified by changing the bias voltage amplitude in the Reset process (Fig. 22(b)). For instance, the initial conductance of the device was first switched to $14.5G_0$. After applying three negative bias voltages with increasing Reset voltage range, the conductance was sequentially reduced from $14.5G_0$ to $8G_0$, $4G_0$, and G_0. Modification of the quantum conductance states in ITO/ZnO/ITO devices were also achieved by changing the compliance current level in the Set process and voltage amplitude in the Reset process as well (Figs. 22(c) and 22(d)). Interestingly, significant current oscillations were also observed in ITO/ZnO/ITO devices during the RS process, as shown in Fig. 23 [80]. The amplitude of the conductance oscillations were found to concentrate at integer values of G_0, implies that the formation/rupture of several monatomic chains contribute to this phenomenon. The well controlled conductance quantization behaviors in oxide-based resistive switching

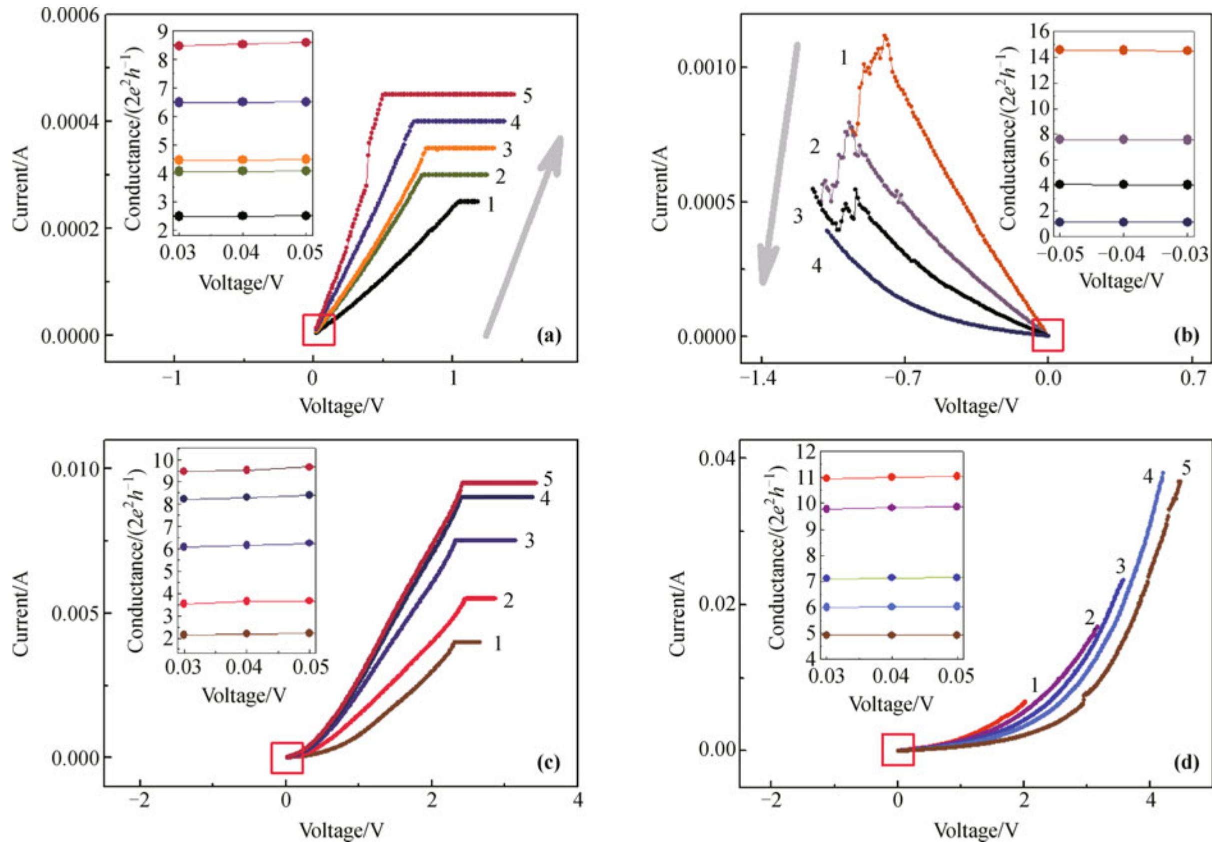

Fig. 22 Current–voltage characteristics of **(a)(b)** an Nb/ZnO/Pt device and **(c)(d)** an ITO/ZnO/ITO device with various current compliances and voltage ranges in the Set and Reset processes, respectively. Inset: Corresponding conductance values read at 0.03, 0.04 and 0.05 V showing that the conductance value is insensitive to the read voltage at low bias. (Reproduced with permission from Ref. [80], Copyright 2012 WILEY-VCH Verlag GmbH & Co. KGaA, Weinheim)

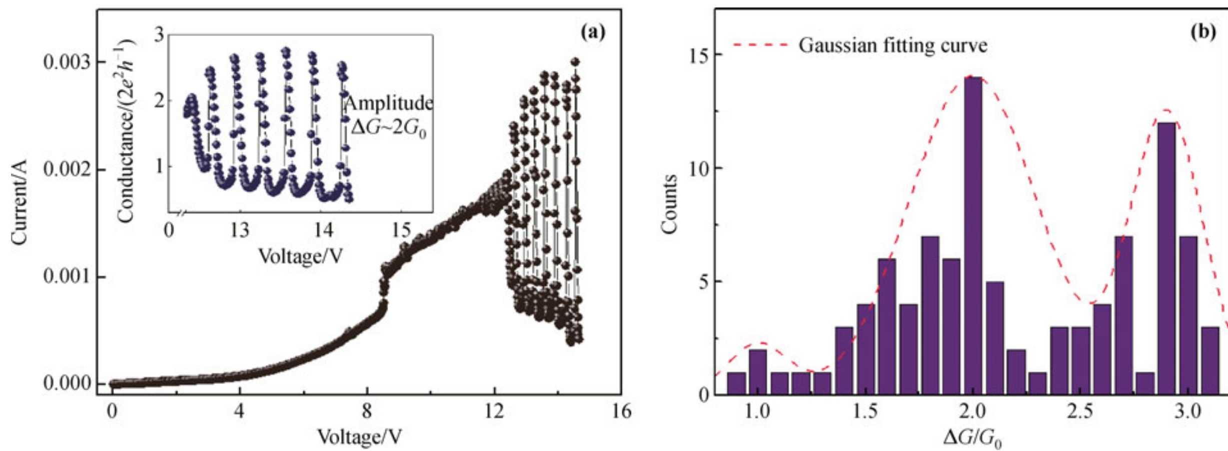

Fig. 23 **(a)** Current oscillations observed during the Set process in an ITO/ZnO/ITO device. Inset: corresponding *G*–*V* curve in a voltage range from 12.3 to 14.4 V. **(b)** Histogram of the oscillation amplitude extracted from 14 curves similar to that in (a). Dotted line: Gaussian fitting curve of the histogram as a guide to the eyes. (Reproduced with permission from Ref. [80], Copyright 2012 WILEY-VCH Verlag GmbH & Co. KGaA, Weinheim)

memories not only could help to achieve multi-level storage for ultrahigh density memory applications, but also could provide a platform to develop new one-dimensional nano-devices based on quantum effects.

6 Summary and outlook

This review mainly describes three aspects. At first, some available approaches to detect and characterize the conducting paths in filamentary model based oxide RRAMs were introduced. Then, the effective methods that can help to improve the RS performances were addressed. These methods facilitate us to deeply understand the RS working mechanism, and provide guidelines from materials selection to structure design perspective to obtain stable RRAMs. In further, the observed quantum conductance behaviors which may help to realize the storage of data at atomic scale were also discussed.

In search of the scalability limit in RRAMs, filamentary model based devices appear to be very promising due to the local switching character. The migration of atoms or electrons in a confined region affects the resistive states of the device seriously. It seems that the ultimate scaling potential could be in atomic scale where the RS can be realized by manipulating only one or several atoms in a monatomic chain that connects the electrodes, though it is very difficult to achieve.

Despite the potential as high density data storage, extensive troublesome issues are still present. For example, the operation currents in RRAMs with unipolar RS characteristics, the Reset process is accomplished with a filaments thermal rupture process. As a consequence, a large current density is always required for Reset process, which directly affects the efficiency for the electrical operations. Another serious problem relies on the variations of operation parameters between cells in the same device. Although many researchers have demonstrated the excellent memory performances such as high switching speed, low operation voltages, good retention, as well as cyclability in different systems, few reports concentrate on the study of the comprehensive RS properties in the same devices are not clearly addressed, but which are highly desired.

Furthermore, many problems will be raised when the devices are integrated into the crossbar matrix for practical application, including the cross talk problem and tunneling induced leakage current. Fortunately, thanks to the contribution of dedicated researchers, approaches to overcome these problems are being solved one by one. It has been proposed that by introducing a diode, the sneak current issue can be solved. On the other hand, dedicated device structure design appears to be another good choice. For electrochemical metallization RS memories, a back-to-back structure which could lead to complementary RS can be employed to prevent the issue as well [85].

In competing with traditional charge-based memories, the RS for digital and analog circuit design is still very young, and faces many challenges. From another perspective, apart from data storage, RS could also find its usage in other fields. For example, it can be used as a switch to replace the relay with complicated structure in some occasions, which need not require so many stringent conditions as memory demands.

Abbreviations

a-Si	amorphous silicon
AZO	Al:ZnO
BFO	$BiFeO_3$
ECM	electrochemical metallization
EDX	energy dispersive X-ray
EELS	electron energy-loss spectroscopy
EFM	electrostatic force microscopy
FeRAM	ferroelectric random access memory
GO	graphene oxide
HRS	high resistive state
HRTEM	high-resolution transmission electron microscopy
KPM	Kelvin probe microscopy
LC-AFM	local current atomic force microscopy
LRS	low resistive state
MIM	metal-insulator-metal
MRAM	magnetic random access memory
PCMO	$Pr_{0.7}Ca_{0.3}MnO_3$
PRAM	phase-change random access memory
RCB	random circuit breaker
RRAM	resistive random access memory
RS	resistive switching
RT	room temperature
SPM	scan probe microscopy
STEM	scanning transmission electron microscopy
TEM	transmission electron microscopy

Acknowledgements This work was supported by State Key Research Program of China (973 Program; Grant Nos. 2009CB930803 and 2012CB933004), National Natural Science Foundation of China, Zhejiang and Ningbo Natural Science Foundations, Chinese Academy of Sciences (CAS), and Science and Technology Innovative Research Team of Ningbo Municipality (Grant Nos. 2011B82004 and 2009B21005).

References

[1] Hickmott T W. Low-frequency negative resistance in thin anodic oxide films. Journal of Applied Physics, 1962, 33(9): 2669–2682

[2] Sutherland R R. A theory for negative resistance and memory effects in thin insulating films and its application to Au–ZnS–Au devices. Journal of Physics D: Applied Physics, 1971, 4(3): 468–479

[3] Hickmott T W. Potential distribution and negative resistance in thin oxide films. Journal of Applied Physics, 1964, 35(9): 2679–2689

[4] Liu S Q, Wu N J, Ignatiev A. Electric-pulse-induced reversible resistance change effect in magnetoresistive films. Applied Physics Letters, 2000, 76(19): 2749–2751

[5] Lai Y-S, Tu C-H, Kwong D-L, et al. Bistable resistance switching of poly(N-vinylcarbazole) films for nonvolatile memory applications. Applied Physics Letters, 2005, 87(12): 122101 (3 pages)

[6] Hu B, Zhuge F, Zhu X, et al. Nonvolatile bistable resistive switching in a new polyimide bearing 9-phenyl-9*H*-carbazole pendant. Journal of Materials Chemistry, 2012, 22(2): 520–526

[7] Jo S H, Kim K H, Lu W. High-density crossbar arrays based on a Si memristive system. Nano Letters, 2009, 9(2): 870–874

[8] Jo S H, Kim K H, Lu W. Programmable resistance switching in nanoscale two-terminal devices. Nano Letters, 2009, 9(1): 496–500

[9] Zhuge F, Dai W, He C L, et al. Nonvolatile resistive switching memory based on amorphous carbon. Applied Physics Letters, 2010, 96(16): 163505 (3 pages)

[10] He C L, Zhuge F, Zhou X F, et al. Nonvolatile resistive switching in graphene oxide thin films. Applied Physics Letters, 2009, 95 (23): 232101 (3 pages)

[11] Jeong H Y, Kim J Y, Kim J W, et al. Graphene oxide thin films for flexible nonvolatile memory applications. Nano Letters, 2010, 10 (11): 4381–4386

[12] Lee M J, Han S, Jeon S H, et al. Electrical manipulation of nanofilaments in transition-metal oxides for resistance-based memory. Nano Letters, 2009, 9(4): 1476–1481

[13] Oka K, Yanagida T, Nagashima K, et al. Nonvolatile bipolar resistive memory switching in single crystalline NiO heterostructured nanowires. Journal of the American Chemical Society, 2009, 131(10): 3434–3435

[14] Yun J-B, Kim S, Seo S, et al. Random and localized resistive switching observation in Pt/NiO/Pt. physica status solidi (RRL) – Rapid Research Letters, 2007, 1(6): 280–282

[15] Guan W, Long S, Liu Q, et al. Nonpolar nonvolatile resistive switching in Cu doped ZrO_2. Electron Device Letters, IEEE, 2008, 29(5): 434–437

[16] Li Y, Long S, Lv H, et al. Improvement of resistive switching characteristics in ZrO_2 film by embedding a thin TiO_x layer. Nanotechnology, 2011, 22(25): 254028

[17] Wang Y, Liu Q, Long S, et al. Investigation of resistive switching in Cu-doped HfO_2 thin film for multilevel non-volatile memory applications. Nanotechnology, 2010, 21(4): 045202

[18] Chan M Y, Zhang T, Ho V, et al. Resistive switching effects of HfO_2 high-*k* dielectric. Microelectronic Engineering, 2008, 85 (12): 2420–2424

[19] Lin K-L, Hou T-H, Shieh J, et al. Electrode dependence of filament formation in HfO_2 resistive-switching memory. Journal of Applied Physics, 2011, 109(8): 084104 (7 pages)

[20] Li S-L, Gang J-L, Li J, et al. Reproducible low-voltage resistive switching in a low-initial-resistance $Pr_{0.7}Ca_{0.3}MnO_3$ junction. Journal of Physics D: Applied Physics, 2008, 41(18): 185409

[21] Gang J-L, Li S-L, Liao Z-L, et al. Clockwise vs counter-clockwise

I–V hysteresis of point-contact metal-tip/$Pr_{0.7}Ca_{0.3}MnO_3$/Pt devices. Chinese Physics Letters, 2010, 27(2): 027301

[22] Yin K, Li M, Liu Y, et al. Resistance switching in polycrystalline $BiFeO_3$ thin films. Applied Physics Letters, 2010, 97(4): 042101 (3 pages)

[23] Yang C H, Seidel J, Kim S Y, et al. Electric modulation of conduction in multiferroic Ca-doped $BiFeO_3$ films. Nature Materials, 2009, 8(6): 485–493

[24] Chen X, Wu G, Zhang H, et al. Nonvolatile bipolar resistance switching effects in multiferroic $BiFeO_3$ thin films on $LaNiO_3$-electrodized Si substrates. Applied Physics A: Materials Science & Processing, 2010, 100(4): 987–990

[25] Szot K, Speier W, Bihlmayer G, et al. Switching the electrical resistance of individual dislocations in single-crystalline $SrTiO_3$. Nature Materials, 2006, 5(4): 312–320

[26] Ni M C, Guo S M, Tian H F, et al. Resistive switching effect in $SrTiO_{3-\delta}$/Nb-doped $SrTiO_3$ heterojunction. Applied Physics Letters, 2007, 91(18): 183502 (3 pages)

[27] Muenstermann R, Menke T, Dittmann R, et al. Coexistence of filamentary and homogeneous resistive switching in Fe-doped $SrTiO_3$ thin-film memristive devices. Advanced Materials, 2010, 22(43): 4819–4822

[28] Garcia V, Fusil S, Bouzehouane K, et al. Giant tunnel electroresistance for non-destructive readout of ferroelectric states. Nature, 2009, 460(7251): 81–84

[29] Jeong W C, Lee B I, Joo S K. Three level, six state multilevel magnetoresistive RAM(MRAM). Journal of Applied Physics, 1999, 85(8): 4782–4784

[30] Wuttig M. Phase-change materials: towards a universal memory? Nature Materials, 2005, 4(4): 265–266

[31] Waser R, Dittmann R, Staikov G, et al. Redox-based resistive switching memories – nanoionic mechanisms, prospects, and challenges. Advanced Materials, 2009, 21(25–26): 2632–2663

[32] Kwon D H, Kim K M, Jang J H, et al. Atomic structure of conducting nanofilaments in TiO_2 resistive switching memory. Nature Nanotechnology, 2010, 5(2): 148–153

[33] Sawa A, Fujii T, Kawasaki M, et al. Hysteretic current–voltage characteristics and resistance switching at a rectifying Ti/$Pr_{0.7}Ca_{0.3}MnO_3$ interface. Applied Physics Letters, 2004, 85 (18): 4073–4075

[34] Dong C Y, Shang D S, Shi L, et al. Roles of silver oxide in the bipolar resistance switching devices with silver electrode. Applied Physics Letters, 2011, 98(7): 072107 (3 pages)

[35] Meijer G I, Staub U, Janousch M, et al. Valence states of Cr and the insulator-to-metal transition in Cr-doped $SrTiO_3$. Physical Review B: Condensed Matter and Materials Physics, 2005, 72 (15): 155102

[36] Maksymovych P, Jesse S, Yu P, et al. Polarization control of electron tunneling into ferroelectric surfaces. Science, 2009, 324 (5933): 1421–1425

[37] Kim S, Jeong H Y, Choi S Y, et al. Comprehensive modeling of resistive switching in the Al/TiO_x/TiO_2/Al heterostructure based on space-charge-limited conduction. Applied Physics Letters, 2010, 97(3): 033508 (3 pages)

[38] Lee M J, Lee C B, Lee D, et al. A fast, high-endurance and scalable non-volatile memory device made from asymmetric Ta_2O_{5-x}/TaO_{2-x} bilayer structures. Nature Materials, 2011, 10(8): 625–630

[39] Schindler C, Meier M, Waser R, et al. Resistive switching in Ag–Ge–Se with extremely low write currents. In: Non-Volatile Memory Technology Symposium, 2007. NVMTS '07, 2007, 82–85

[40] Guan W, Liu M, Long S, et al. On the resistive switching mechanisms of Cu/ZrO_2:Cu/Pt. Applied Physics Letters, 2008, 93 (22): 223506 (3 pages)

[41] Kim K M, Jeong D S, Hwang C S. Nanofilamentary resistive switching in binary oxide system; a review on the present status and outlook. Nanotechnology, 2011, 22(25): 254002

[42] Chang S H, Chae S C, Lee S B, et al. Effects of heat dissipation on unipolar resistance switching in Pt/NiO/Pt capacitors. Applied Physics Letters, 2008, 92(18): 183507 (3 pages)

[43] Larentis S, Cagli C, Nardi F, et al. Filament diffusion model for simulating reset and retention processes in RRAM. Microelectronic Engineering, 2011, 88(7): 1119–1123

[44] Waser R, Aono M. Nanoionics-based resistive switching memories. Nature Materials, 2007, 6(11): 833–840

[45] Zhu X, Zhuge F, Li M, et al. Microstructure dependence of leakage and resistive switching behaviours in Ce-doped $BiFeO_3$ thin films. Journal of Physics D: Applied Physics, 2011, 44(41): 415104

[46] Zuo Q, Long S, Liu Q, et al. Self-rectifying effect in gold nanocrystal-embedded zirconium oxide resistive memory. Journal of Applied Physics, 2009, 106(7): 073724 (5 pages)

[47] Sim H, Seong D-J, Chang M, et al. Excellent resistance switching characteristics of Pt/single-crystal Nb-doped SrTiO3 Schottky junction. In: 21st Non-Volatile Semiconductor Memory Workshop, 2006. IEEE NVSMW 2006, 88–89

[48] Li M, Zhuge F, Zhu X, et al. Nonvolatile resistive switching in metal/La-doped $BiFeO_3$/Pt sandwiches. Nanotechnology, 2010, 21(42): 425202

[49] Zhuge F, Hu B, He C, et al. Mechanism of nonvolatile resistive switching in graphene oxide thin films. Carbon, 2011, 49(12): 3796–3802

[50] Bid A, Bora A, Raychaudhuri A K. Temperature dependence of the resistance of metallic nanowires (diameter $\geqslant$ 15 nm): Applicability of Bloch-Grüneisen theorem. Physical Review B:

Condensed Matter and Materials Physics, 2006, 74(3): 035426 (9 pages)

[51] Guo Y, Zhang Y F, Bao X Y, et al. Superconductivity modulated by quantum size effects. Science, 2004, 306(5703): 1915–1917

[52] Koch C C, Scarbrough J O, Kroeger D M. Effects of interstitial oxygen on the superconductivity of niobium. Physical Review B: Condensed Matter and Materials Physics, 1974, 9(3): 888–897

[53] Son J Y, Shin Y H. Direct observation of conducting filaments on resistive switching of NiO thin films. Applied Physics Letters, 2008, 92(22): 222106 (3 pages)

[54] Chae S C, Lee J S, Kim S, et al. Random circuit breaker network model for unipolar resistance switching. Advanced Materials, 2008, 20(6): 1154–1159

[55] Zhuge F, Peng S, He C, et al. Improvement of resistive switching in Cu/ZnO/Pt sandwiches by weakening the randomicity of the formation/rupture of Cu filaments. Nanotechnology, 2011, 22(27): 275204

[56] Lee M H, Hwang C S. Resistive switching memory: observations with scanning probe microscopy. Nanoscale, 2011, 3(2): 490–502

[57] Choi S J, Park G S, Kim K H, et al. *In situ* observation of voltage-induced multilevel resistive switching in solid electrolyte memory. Advanced Materials, 2011, 23(29): 3272–3277

[58] Cho B, Yun J M, Song S, et al. Direct observation of Ag filamentary paths in organic resistive memory devices. Advanced Functional Materials, 2011, 21(20): 3976–3981

[59] Yang Y C, Pan F, Liu Q, et al. Fully room-temperature-fabricated nonvolatile resistive memory for ultrafast and high-density memory application. Nano Letters, 2009, 9(4): 1636–1643

[60] Yao J, Sun Z, Zhong L, et al. Resistive switches and memories from silicon oxide. Nano Letters, 2010, 10(10): 4105–4110

[61] Sakamoto T, Lister K, Banno N, et al. Electronic transport in Ta_2O_5 resistive switch. Applied Physics Letters, 2007, 91(9): 092110 (3 pages)

[62] Park G S, Li X S, Kim D C, et al. Observation of electric-field induced Ni filament channels in polycrystalline NiO_x film. Applied Physics Letters, 2007, 91(22): 222103 (3 pages)

[63] Tsuruoka T, Terabe K, Hasegawa T, et al. Forming and switching mechanisms of a cation-migration-based oxide resistive memory. Nanotechnology, 2010, 21(42): 425205

[64] Terabe K, Hasegawa T, Nakayama T, et al. Quantized conductance atomic switch. Nature, 2005, 433(7021): 47–50

[65] Guo X, Schindler C, Menzel S, et al. Understanding the switching-off mechanism in Ag^+ migration based resistively switching model systems. Applied Physics Letters, 2007, 91(13): 133513 (3 pages)

[66] Liu Q, Sun J, Lv H, et al. Real-time observation on dynamic growth/dissolution of conductive filaments in oxide-electrolyte-based ReRAM. Advanced Materials, 2012, 24(14): 1844–1849

[67] Yang Y, Gao P, Gaba S, et al. Observation of conducting filament growth in nanoscale resistive memories. Nature Communications, 2012, 3: 732

[68] Peng S, Zhuge F, Chen X, et al. Mechanism for resistive switching in an oxide-based electrochemical metallization memory. Applied Physics Letters, 2012, 100(7): 072101 (4 pages)

[69] Liu Q, Long S, Lv H, et al. Controllable growth of nanoscale conductive filaments in solid-electrolyte-based ReRAM by using a metal nanocrystal covered bottom electrode. ACS Nano, 2010, 4 (10): 6162–6168

[70] Lee W, Jung H J, Lee M H, et al. Oxygen surface exchange at grain boundaries of oxide ion conductors. Advanced Functional Materials, 2012, 22(5): 965–971

[71] Park C, Jeon S H, Chae S C, et al. Role of structural defects in the unipolar resistive switching characteristics of Pt/NiO/Pt structures. Applied Physics Letters, 2008, 93(4): 042102 (3 pages)

[72] Zou C, Chen B, Zhu X-J, et al. Local leakage current behaviours of $BiFeO_3$ films. Chinese Physics B, 2011, 20(11): 117701

[73] Park J-W, Park J-W, Jung K, et al. Influence of oxygen content on electrical properties of NiO films grown by rf reactive sputtering for resistive random-access memory applications. Journal of Vacuum Science and Technology B: Microelectronics and Nanometer Structures, 2006, 24(5): 2205–2208

[74] Bae Y C, Lee A R, Kwak J S, et al. Dependence of resistive switching behaviors on oxygen content of the Pt/TiO_{2-x}/Pt matrix. Current Applied Physics, 2011, 11(2): e66–e69

[75] Zhang H, Liu L, Gao B, et al. Gd-doping effect on performance of HfO_2 based resistive switching memory devices using implantation approach. Applied Physics Letters, 2011, 98(4): 042105 (3 pages)

[76] Liu Q, Long S, Wang W, et al. Improvement of resistive switching properties in ZrO_2-based ReRAM with implanted Ti ions. Electron Device Letters, IEEE, 2009, 30(12): 1335–1337

[77] Fang Z, Yu H Y, Liu W J, et al. Temperature instability of resistive switching on HfO_x-based RRAM devices. Electron Device Letters, IEEE, 2010, 31(5): 476–478

[78] Goux L, Czarnecki P, Chen Y Y, et al. Evidences of oxygen-mediated resistive-switching mechanism in TiN\HfO_2\Pt cells. Applied Physics Letters, 2010, 97(24): 243509 (3 pages)

[79] Tsuruoka T, Terabe K, Hasegawa T, et al. Effects of moisture on the switching characteristics of oxide-based, gapless-type atomic switches. Advanced Functional Materials, 2012, 22(1): 70–77

[80] Zhu X, Su W, Liu Y, et al. Observation of conductance quantization in oxide-based resistive switching memory. Advanced Materials, 2012, DOI: 10.1002/adma.201201506

[81] Ohnishi H, Kondo Y, Takayanagi K. Quantized conductance through individual rows of suspended gold atoms. Nature, 1998,

395(6704): 780–783
[82] Seo J W, Park J W, Lim K S, et al. Transparent resistive random access memory and its characteristics for nonvolatile resistive switching. Applied Physics Letters, 2008, 93(22): 223505 (3 pages)
[83] Li C Z, He H X, Bogozi A, et al. Molecular detection based on conductance quantization of nanowires. Applied Physics Letters, 2000, 76(10): 1333–1335
[84] Shu C, Li C Z, He H X, et al. Fractional conductance quantization in metallic nanoconstrictions under electrochemical potential control. Physical Review Letters, 2000, 84(22): 5196–5199
[85] Linn E, Rosezin R, Kügeler C, et al. Complementary resistive switches for passive nanocrossbar memories. Nature Materials, 2010, 9(5): 403–406